IOP Publishing Quantum Sci. Technol. 11 (2026) 013001 https://doi.org/10.1088/2058-9565/ae30a5

Quantum Science and Technology

TOPICAL REVIEW

Recent progress on mid-infrared single-photon detectors and sources for satellite-based quantum key distribution—a review

Liam Flannigan[1,*], Mostafa Khalil[2], Phyllis Chiu[1] and Chang-qing Xu[1]

[1] Department of Engineering Physics, McMaster University, Hamilton, Canada
[2] Department of Electrical and Software Engineering, Schulich School of Engineering, Calgary, Canada
* Author to whom any correspondence should be addressed.

E-mail: flannilg@mcmaster.ca

Keywords: quantum key distribution, mid-infrared, detectors, sources

OPEN ACCESS

RECEIVED
30 July 2025

REVISED
1 December 2025

ACCEPTED FOR PUBLICATION
23 December 2025

PUBLISHED
20 January 2026

Abstract

Satellite quantum key distribution technology has developed rapidly using near-infrared wavelengths and is expected to enable global quantum communication. However, link availability is still hampered by detrimental effects in the free-space channel, such as background noise from solar radiation and attenuation from turbulence and weather such as haze and fog. One potential mitigation technique is to move to the mid-infrared atmospheric transmission window (3–5 μms) where background noise and turbulence effects are significantly reduced. While mid-infrared quantum technology is not as well developed, advancements in mid-infrared entangled photon pair generation and nonlinear upconversion single-photon detectors could be poised to enable daytime satellite downlinks with increased reliability. This review compares the state of the art for quantum transmitters and receivers in the mid-infrared to the more established near-infrared technology. The goal is to identify gaps in transmitter and/or receiver technology in the mid-infrared, and to determine if the mid-infrared can offer significant advantages over the near infrared for quantum communication.

1. Introduction

Quantum technologies have developed rapidly in recent years. It is clear to see why, given myriad applications of both quantum sources and single-photon detectors (SPDs): quantum computing [1, 2], quantum imaging [3], free-space quantum communications [4–6], military applications such as surveillance and reconnaissance [7], quantum information theory [8], quantum metrology [9, 10], and more. One application in particular has been a focus of research and development efforts across the globe—quantum key distribution (QKD). QKD involves the transmission of a secret keys through an insecure channel by using quantum-mechanical information carriers [11]. There have been numerous developments in both fiber-based and free-space quantum communication links for the purpose of transmitting these secret keys. Despite continuous record-breaking experiments for fiber-based QKD, the lack of quantum state amplification places upper limits on the feasibility of a global fiber network for QKD [12]. As an alternative, the relatively low attenuation of the free-space channel in specific atmospheric transmission windows means that space-based QKD is promising for creating a global quantum information system. Since the launch of China's Micius satellite and the successful demonstration of QKD with a ground station in 2017, there has been significant effort aimed at further developing space-based QKD demonstrations [13, 14]. Canada is planning the Quantum Encryption and Science Satellite (QEYSSat), and Germany has worked with Canada to demonstrate QKD between airplanes and ground stations [15, 16]. All the while China has continued to innovate in this space, with QKD demonstrations during both daytime and nighttime conditions over long distance free-space channels [17–19]. There have been several successful satellite-based QKD demonstrations as well. These include QUESS, Tiangong-2, and Jinan-1 from China, SpooQy-1 from Singapore, and QUBE from Germany [20–24]. There are also a number of planned demonstrations, including Canada's QEYSSat and ESA's Eagle-1 missions in the near

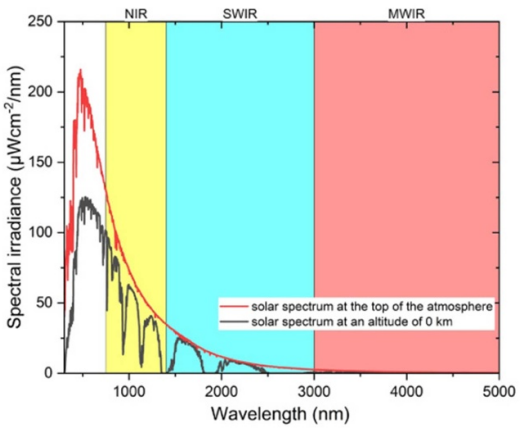

Figure 1. Solar irradiance versus wavelength at sea level (red) and in the upper atmosphere (blue). The atmospheric windows are denoted by the shaded regions: near infrared (NIR), yellow; short-wave infrared (SWIR), cyan; mid-wave infrared (MWIR), red. Reproduced from [31]. CC BY 4.0.

future [16, 25]. This makes it clear that space based QKD will continue to be developed in earnest in the coming decade.

The typical configuration for space-based QKD is a satellite downlink due to the lower losses associated with this configuration. Currently, the most common wavelengths for transmission are the near-infrared at around 750–820 nm and, more recently, the short-wave infrared at 1550 nm which resides in the C-band commonly used for terrestrial telecommunications. Entangled photon sources are readily available for both wavelengths, as spontaneous parametric down conversion (SPDC) has been demonstrated producing entangled photon pairs for both cases [26–28]. There is some debate over which of these wavelengths is optimal for QKD. For example, 1550 nm is attractive because of the wide availability of sensitive C-band SPDs and high-quality off-the-shelf components compatible with this wavelength due to decades of telecoms research and development. Additionally, the wavelength dependent nature of scattering and atmospheric turbulence tends to suggest that longer wavelengths will be exposed to less of both these detrimental effects in general [29]. However, using spatial filtering, adaptive optics, and considering the improved optical coupling of shorter wavelengths into transmission and receiving telescopes, and the higher performance of off-the-shelf silicon avalanche photodiodes suggests 775 nm is a better wavelength to work with [30]. As illustrated in figure 1, the spectral irradiance as a function of wavelength drops sharply as wavelength increases through the atmospheric transmission windows, which suggests longer wavelengths could have larger signal-to-noise values due to the reduction in background radiation. There are arguments to be made for both wavelengths, but both have been used to demonstrate long distance QKD, and they will undoubtedly serve as the backbone of QKD demonstrations in space for the next 5–10 years.

There is also growing interest in developing longer wavelength photon sources and SPDs for free-space QKD. The next atmospheric transmission window after the short-wave infrared is the mid-infrared (3–5 μms), and it has promise for QKD links. One motivation for using the mid-infrared is that theory suggests that the effects of fog, turbulence, and scattering are mitigated at longer wavelengths [32–34]. This could lead to higher link availability compared to the shorter wavelengths currently in use. Another potential benefit is the reduction in background noise for the atmospheric channel. It is well known that the use of single photons as qubits prevents us from increasing the signal-to-noise ratio (SNR) by increasing the signal power, and only the photon generation rate can change [35]. The only way to increase the SNR is to reduce the noise. It has been shown previously that spectral radiance (which is used to calculate background channel noise) is much lower in the mid-infrared compared to the near and short wave infrared [30, 36]. So, if mid-infrared photon sources and SPDs can reach parity with the shorter wavelength technology, there is reason to believe the mid-infrared could allow for improved QKD links. That is not to say there would be no drawbacks to using the mid-infrared. The dependence of diffraction-based losses for free-space propagation is linear with respect to wavelength. So, longer wavelengths will have increased free-space losses assuming telescope sizes are held constant. This can be compensated for by increasing both transmit and receive telescope size, but this comes with a proportionate increase in the cost of the satellite payload itself. This can help explain the current preference for shorter wavelengths.

The idea to use longer wavelengths is not new for QKD, as Temperao *et al* performed one of the earliest feasibility studies for mid-infrared QKD in 2008 [37]. The study implemented the BB84 protocol using 4.6 μm light from a quantum cascade laser as the source, and an upconversion module based on sum frequency generation for the receiver. The results were compared to a typical 780 nm system, showing that in clear atmospheric conditions, the 780 nm source outperformed the mid-infrared one. However, as visibility decreased, there was a tipping point where the 4.6 μm link outperformed the shorter wavelength. At the time, high quality mid-infrared photon sources and sensitive mid-infrared SPDs were not available. The main reason upconversion was used (and is still in use today) is that it is typically more efficient to convert the longer wavelength mid-infrared photons into the range of peak sensitivity for silicon avalanche photodiodes than it is to use a direct mid-infrared detector. Since Temperao's study, there have been a few investigations into using terahertz frequencies for QKD, but a detailed investigation of the state-of-the-art for mid-infrared technology for QKD applications has not been performed since [38, 39]. There have been significant improvements in both mid-infrared single-photon sources and SPDs. For the former, quantum and interband cascade lasers as well as SPDC sources have made significant strides. Meanwhile, supercooled nanowire SPDs (SNSPDs) have emerged as a promising SPD for a wide range of wavelengths, and upconversion SPDs have continued to improve as well.

This brings us to the goal of this review article. The aim of this review is to catalog the current state of the art of mid-infrared transmitter and receiver technology relevant to QKD. The mid-infrared state-of-the-art will be compared to the state-of-the-art in near and short infrared wavelengths to determine how close the mid-infrared is to parity with this technology. Finally, any gaps or interesting research opportunities in the coming decade will be identified, and a recommendation on the overall potential of the mid-infrared for QKD will be made. The review will cover the state of the art for SPDs in section 2, single-photon sources in section 3, and a closing discussion and conclusion in section 4. Sections 2 and 3 will end with tables comparing the state-of-the-art for each wavelength range under consideration using the relevant figures of merit. We hope that this will aid in guiding research efforts on mid-infrared technologies for QKD applications in the near future.

2. SPDs

2.1. Near-infrared detector state-of-the-art

Before covering the various mid-infrared SPDs, it is important to set a benchmark to compare them to. In this section, we briefly cover the state-of-the-art for current near-infrared SPD technology, to be included in the comparison table at the end of this section. It is important to note that this section will not be as in-depth as the following section on mid-infrared technology. This is due to the fact that near-infrared detectors are already well-established as the best current technology for single-photon detection, which is why the vast majority of the available literature focuses on the 450–950 nm band for use with silicon detectors and telecoms C-band to leverage high quality commercial-off-the-shelf components. For those interested in more in-depth coverage of near-infrared SPDs, there are several high quality reviews that have been published on the matter from the last few years [31, 40–43].

There are two main technologies to consider when discussing near-infrared SPDs: direct detection via single-photon avalanche photodiodes (SPADs) and SNSPDs. SPADs are avalanche photodiodes reverse biased above the breakdown voltage (known as Geiger mode operation), so that the electron-hole pairs generated by photon absorption are multiplied in an avalanche gain process [9]. There are several figures-of-merit for a SPD that will be introduced prior to the discussion to follow. The first is the system detection efficiency (SDE). This is a combination of the internal quantum efficiency of the detector itself, the photon absorption efficiency, and the optical coupling efficiency for coupling photons into the system. The internal quantum efficiency represents the probability that an absorbed photon creates an output electrical signal. The photon absorption efficiency is the probability that an incident photon is absorbed in the detector, and the optical coupling efficiency represents how well a photon incident on the input aperture of the detector is coupled onto its single-photon sensitive area [44]. The photon absorption efficiency also depends on the polarization of the light, as polarization parallel to the nanowire maximizes absorption, while perpendicular polarization represents the minimum absorption efficiency. Another important figure-of-merit is the dark count. Dark count refers to a false detection event in a SPD that occurs in the absence of any incident photons. Their physical origin can be tied to various noise sources like thermal excitation of charge carriers, tunneling or leakage currents, ambient thermal radiation, and cosmic rays. Dark counts are typically given in counts-per-second (cps) or Hertz (Hz) and can be reduced by cooling the detector and using narrow optical band filters to reduce unwanted incident radiation. Single photon avalanche photodiodes also have to consider afterpulsing,

i.e. false counts after a triggered detection event. Afterpulsing is caused by the release of trapped charge carriers in SPADs during the recovery period following an avalanche event. The afterpulse probability quantifies the likelihood of an afterpulse per detection, and afterpulsing can be mitigated by modifying the cooling temperature, the detector's quenching electronics, and the dead time. The dead time is the period following a detection event during which the detector is insensitive to subsequent photons. It is a function of the time required for avalanche quenching, carrier trap relaxation, and circuit recovery time. The dead time limits the maximum count rate and can distort photon statistics in high-rate QKD systems. Typical dead times range from tens of nanoseconds in SPADs to sub-nanosecond scales in SNSPDs. Another figure-of-merit is the timing jitter, which denotes the uncertainty in the recorded arrival time of a photon relative to its actual arrival. Its physical origin lies in variations in avalanche buildup time, electronic noise, and signal processing delays. Low timing jitter is vital for QKD systems due to the requirement for precise time-bin encoding and coincedence detection. Typical values are tens of picoseconds for SNSPDs and hundreds of picoseconds for SPADs. SPDs can be operated in gated or continuous mode as well. In continuous mode, the detector is sensitive to photons at all times, which can be useful for high-rate QKD systems. In gated mode, the detector is periodically biased above its breakdown threshold only during pre-specified time windows (gates) that are synchronized with the expected photon arrival times. This can greatly cut down on both dark counts and afterpulsing probabilities, at the cost of limiting the temporal response. Gated detectors must also optimize the gate width, which is the window during which the detector is sensitive to photons in time. Narrower gate widths further reduce dark counts and afterpulsing, while wider gates improve detection probability at the cost of increased noise [9].

Starting with SPADs, the two most popular semiconductor materials are silicon (for the 700–900 nm range) and InGaAs/InP for the telecoms bands [41, 45]. While silicon tends to be the best performer in terms of noise characteristics, speed, sensitivity, and cost, it is large bandgap prevents it from being used for wavelengths $>$1000 nm, necessitating alternative materials such as InGaAs/InP. Si SPADs are readily available off-the-shelf with system detection efficiencies $>$65% for sensitive quantum free-space communication applications [41, 46–49]. InGaAs/InP has also demonstrated excellent performance, with detection efficiencies in the range of 55%–60% at 1550 nm, although generally with higher dark count rates (DCRs) than observed in Silicon even with cooling [50–52]. The lower noise and higher temperature operation threshold for silicon SPDs has also led to investigations in using frequency upconversion to convert telecom wavelength photons at 1550 to wavelengths in the sensitivity range of silicon SPADs (600–800 nm). The general conclusion seems to be upconversion is highly promising for quantum applications in the telecom band as well, with improved communication rates and larger communication distances versus direct detection using InGaAs [51, 53]. These SPADs are the current gold standard for room temperature and Peltier-cooled operation and will serve as a useful benchmark for similar technology in the mid-infrared.

SNSPDs are the other main technology for near-infrared single-photon detection. SNSPDs are made of various superconducting materials, with common choices being NbN, NbTiN, WSi, and MoSi [52]. SNSPDs offer several advantages over semiconductor SPADs, with the most relevant to his review being extremely low dark counts (in some cases $<$1 per day), demonstrated system detection efficiencies $>$90%, broad wavelength ranges for photon absorption, no gating required, low timing jitter, and a short recovery time [54]. Couteau *et al* provided a comprehensive review of detecting telecom wavelength photons using SNSPDs in 2021, showing that many of the materials listed above have demonstrated near-unity system detection efficiencies [55]. The main disadvantages relative to SPADs are the complexity and cost of manufacturing, and the need to operate at cryogenic temperatures, typically $<$10 K [52, 55, 56]. As a result, SNSPDs generally offer the best performance from an SDE standpoint but increase the cost and complexity of the detection assembly versus a comparable SPAD set-up. Which option is better will depend heavily on the target application, and there is no clear best option when it comes to single-photon detection. Representative values for state-of-the-art near-infrared SPDs can be found in a summary table in section 2.3 below. This table includes the results for near-infrared and mid-infrared detectors reviewed in this document and is meant to serve as a quick summary of some of the important metrics to quickly compare the capabilities of these SPD technologies in both wavelength ranges.

2.1.1. Detector cooling technology

This section will briefly review the cooling technology used for modern SPDs. While this section concerns the near-infrared state-of-the-art, this technology is also used for the mid-infrared technology in section 2.2, and this topic is simply best introduced here due to its relevance across both wavelength bands. Cooling technologies play a critical role in the performance of SPDs, as thermal noise influences

both DCRs and timing stability. For SPADs, moderate cooling is typically sufficient to suppress thermally generated carriers that contribute to dark counts. These devices are most commonly cooled using thermoelectric (Peltier) modules, which can maintain operating temperatures between −20 °C and −80 °C depending on the detector design. Peltier cooling offers a compact, solid-state solution compatible with portable or field-deployed QKD systems, though further temperature reduction becomes inefficient due to limited heat-pumping capacity and power consumption. For example, commercial SPAD arrays specify built-in Peltier cooling to reduce DCRs and achieve timing jitter <120 ps [57, 58]. In contrast, superconducting nanowire SPDs require cryogenic cooling to maintain superconductivity, typically <3 Kelvin. These temperature are achieved using closed-cycle cryocoolers, such as the Gifford-McMahon Cryocooler, which are reliable and stable over long-term operation [59, 60]. Laboratories may also make use of hybrid cryocoolers to reach <1.5 K, such as this combination of a pulse tube cryocooler and a Joule–Thompson cryocooler [61]. Many modern superconducting nanowrie detectors make use of compact cryogen-free cryostats that integrate fiber coupling and readout electronics while keeping the total device size manageable for practical applications [62]. While a review of the various cryo-coolers and peltier coolers are beyond the scope of this review, it is important to point out that the choice of cooling technology will come down to the temperature requirements, system complexity, and deployment constraints of the QKD system.

2.2. Types of mid-infrared SPDs

2.2.1. Superconducting nanowire detectors

Although much of the research focus is on visible-NIR wavelengths, SNSPDs are also capable of operation in the mid-infrared thanks to recent advances in device geometry and material selection. The operating principles remain the same as when operating in the NIR: a thin film (2–5 nm) of superconducting material is patterned into a nanowire (50–200 nm width typ.) that covers a substrate, creating the active area of the detector [56, 63]. The nanowire is held at a DC bias just below its critical current and cooled to just below the superconductivity temperature for the material. When an incident photon is absorbed, this leads to a hot-spot on the nanowire, which becomes resistive, causing an output voltage spike. After the nanowire cools off, it returns to its superconducting state and is ready to detect another photon. The coupling efficiency will depend on whether the detector is free-space coupled or fiber coupled, and this is especially important in the mid-infrared as this requires different fiber technology than what is used in the near-infrared.

There are several commonly used superconducting materials for SNSPDs: Niobium Nitride (NbN), Niobium titanium nitride (NbTiN), tungsten silicide (WSi), and molybdenum silicide (MoSi) [64]. NbN is a popular material in the NIR due to its high superconductivity temperature (up to 6 K), and has achieved near 100% detection efficiencies at telecom wavelengths, as well as GHz count rates (with a drop in SDE to <45% at such high speeds) due to its fast recovery time [53, 65, 66]. However, although NbN can detect mid-infrared wavelengths, the SDE at wavelengths longer than 1.5 μm was initially poor. This was first addressed by Korneev *et al* in 2012, where they demonstrated that reducing the strip width of the NbN SNSPD to 40 nm increased SDE at longer wavelengths, and observed measurable signals for wavelengths as long as 10.6 μm [67]. Marsili *et al* built on this result, carrying out a systematic study of the dependence on SDE as a function of nanowire width [68]. The best mid-IR performance was found to be a SDE of 2.6%–5.5% between wavelengths 0.5–5.0 μm, with the efficiency decreasing with increasing wavelength. This represented a significant improvement in mid-IR performance at the time, although it was not without drawbacks. Reducing the nanowire width was more difficult from a manufacturing standpoint, reducing repeatability. Additionally, the DCRs were found to increase by up to two orders of magnitude over typical values with lower nanowire width, reducing SDE due to the increase in noise [69]. Typical values are <100 counts per second (cps) although some devices have demonstrated rates as low as 1 count per day. More recently, this has been improved upon significantly, with Pan *et al* reporting unity internal detection efficiency from 1.5–4.0 μm using NbN via a 62 nm wide nanowire. The overall SDE at 2.95 μm was 32.5%, and was able to obtain measurable responses for wavelengths as long as 10 μm using a narrower 42 nm nanowire [70].

Another promising mid-IR superconducting material is NbTiN, with Chang *et al* using 50 nm wide and 5–9.5 nm thick nanowires to achieve >70% SDE with <15 ps time resolution at 2 μm, as well as internal quantum efficiency of 80% at 4 μm in 2022 [60]. More recently, Ma *et al* further improved on the NbTiN platform by increasing the nitrogen content and deposition pressure, leading to improved performance of 7 nm thick, 55 nm wide films with saturated SDE (approaching 90%) at 2 μms [71]. A 2022 review of NbTiN nanowire timing jitter dependence on wavelength from Taylor *et al* shows that, while jitter increases with increasing wavelength from 1.56–3.5 μm, the jitter is still quite good with a maximum of 30.3 ps at the longest wavelength tested [72]. To date, the best NbTiN SNSPD performance

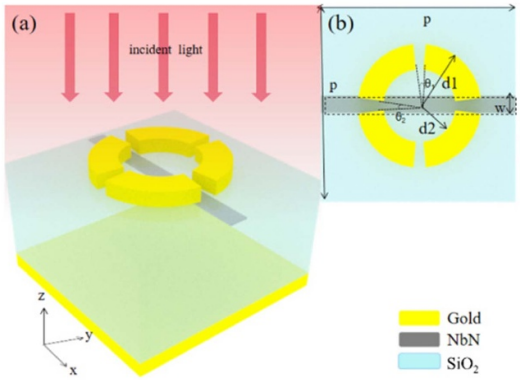

Figure 2. A diagram of the PFSR-SNSPD unit fabricated by Gu *et al*. (a) Illustrates a plane wave vertically incident on the PFSR-SNSPD with the gold ring resonator on top. (b) Is a more detailed diagram showing each segment of the FSRR spanning 80.25°, $\theta\_1 = 5.5°$, $\theta\_2 = 14°$, and the outer and inner radii as d1 and d2, respectively. The nanowire of width w is located within and below the FSRR. The gold mirror on the bottom serves as a reflector to form a cavity for enhanced absorption. Reproduced from [76]. CC BY 4.0.

was presented by China *et al* in 2023 using 7 nm thick NbTiN and wire widths of 60 and 80 nm [73]. They achieved unity internal detection efficiency, as well as a SDE of 84.1% at 2 μm. Although overall SDE does tend to degrade as wavelength increases, these values are promising for extending NbTiN usage into the mid-infrared.

There have also been advances in device structure to mitigate the significant polarization sensitivity of SNSPDs. In 2022, Karl *et al* demonstrated >90% polarization-independent absorption at 1140 nm using a circular design as well as a modified meander design and surface plasmon resonance to reduce polarization sensitivity significantly [74]. Fractal designs have also demonstrated the ability to almost remove polarization insensitivity, with a recent SNSPD from Hao *et al* demonstrating SDE as high as 96% at 930–940 nm with a polarization sensitivity of 1.02. Polarization sensitivity is the ratio of the maximum efficiency to the minimum efficiency as a function of polarization, which was 95/93 in Hao's work [75]. There has also been progress in reducing polarization sensitivity with relatively easy to manufacture device structures. Recently, Gu *et al* demonstrated a polarization-insensitive NbN detector at 1550 nm with a unique periodic four-split ring design [76]. This structure uses surface plasmon resonance to increase the electric field intensity around the nanowire by placing it in the near-field region of the split-ring resonator and aligning it along the gap direction. The response can be tuned by changing the inner and outer ring diameters as well as the four gap angles. This resulted in absorption efficiencies >88% for both TE and TM polarizations incident on the device. The novel structure is shown in figure 2. Thus, NbTiN and NbN are promising materials for relatively high temperature operation SNSPDs in the mid-infrared, and the issues of polarization sensitivity and coupling efficiency are improving significantly with recent advances.

Outside of the Nb family of superconductors, the other superconductors previously mentioned (WSi and MoSi) are also suitable options for mid-infrared detection. There are some trade-offs to consider when using these materials [47, 77, 78]. On the positive side, WSi and MoSi lack grain boundaries like NbN and NbTiN, which allows for larger nanowires and simpler fabrication versus the Nb-based options. On the negative side, the operating temperature is typically an order of magnitude lower than that of the Nb family, ranging from 0.08–0.85 K. Dark counts are comparable, typically in the <100 cps range. WSi has demonstrated unity quantum efficiencies out to 1900 nm, and the record SDE is 93% at 1550 nm by Baek *et al* at an operating temperature of 0.12 K [79–81]. In the mid-infrared, Verma *et al* demonstrated single-photon detection with WSi out to 10 μm and demonstrated saturated internal detection efficiency at a temperature of 0.85 K, although the SDE was not reported [82]. More recently, Hampel *et al* demonstrated a 64 pixel array of WSi SNSPDs capable of single-photon imaging with a DCR <1000 cps operating at a temperature of 350 mK [83]. The device reaches saturated internal efficiency from 3.4–5.3 μm, but a response was measured out to 10 μm. While the experimental SDE is not presented, they reported that internal simulation work indicated >50% SDE over a 1-micron bandwidth for a single pixel. The photon count rate and DCR of the array can be seen below in figure 3. WSi SNSPDs have even been reported operating in the 10–29 μm range, which constitute the long infrared [84]. Given the rapid improvement in overall SDE and the wide wavelength range, WSi is a promising material for mid-infrared single-photon detection. MoSi is also promising for mid-infrared detection,

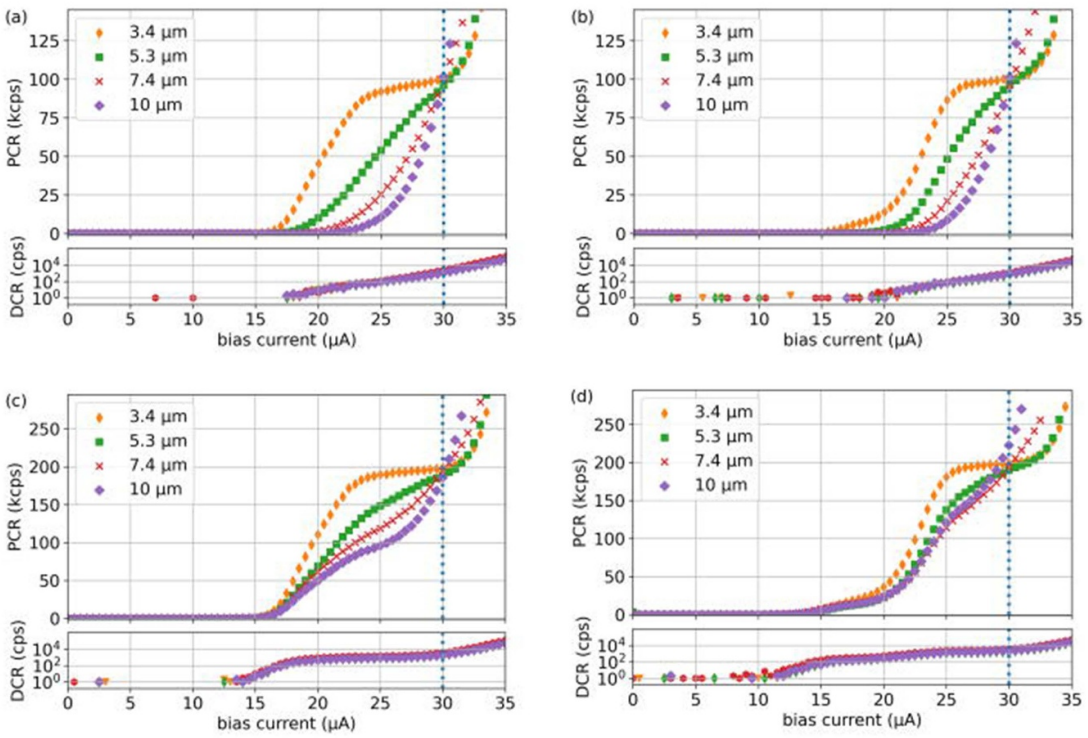

Figure 3. Photon count rate (PCR) and dark count rate (DCR) in counts per second. Panels (a) and (c) represent measurements on the row transmission line with the row bias varied and the columns unbiased and biased at 30 μA, respectively. Panels (b) and (d) show measurements for the column transmission line with column bias varied and the rows unbiased and biased at 30 μA, respectively. Reproduced from [83]. CC BY 4.0.

and saturated detection efficiency was demonstrated by Chen *et al* from 1.55–5.07 μm using MoSi, with dark counts of 10–100 cps and an operating temperature of 0.085 K [85]. Liu *et al* also recently demonstrated a MoSi SNSPD that was relatively insensitive to polarization using a fill factor of 40% for the nanowires [86]. The highest reduction in polarization sensitivity was demonstrated using MoSi nanowires as well, via the use of fractal nanowire patterns, with 95% SDE at 1550 nm regardless of polarization [87]. However, compared to the materials discussed above, there is not as much literature available on mid-infrared SNSPDs using MoSi. One potential reason could be the relatively low operating temperature in the tens of millikelvin. There have been recent advances in higher operating temperature SNSPDs using novel materials such as 2D cuprate superconductors, MgB_2 recently as well, with operating temperatures as high as 25 K [88–90]. In conclusion, given the rapid development of mid-infrared SNSPDs in the last decade, it is clear to see they are one of the leading technologies for mid-infrared single-photon counting and will only continue to improve.

2.2.2. Avalanche photodiodes and upconversion detectors

As with the near-infrared, one of the more promising SPD technologies in the mid-infrared is the use of avalanche photodiodes operating in Geiger-mode (SPADs). However, there are some technical hurdles specific to direct mid-infrared detection that introduce new problems to be solved. Direct mid-infrared detection requires different materials and device configurations from those for NIR. Common choices are bulk HgCdTe, InSb, and more novel structures such as type-2 superlattices and two-dimensional materials like AlAsSb/GaSb, Black Phosphorous (BP)/InSe, MoS_2, and WSe_2 [91–94]. These materials have been previously identified as promising candidates for mid-infrared SPADs and have achieved respectable performance: a state-of-the-art BP/InSe SPAD achieved a responsivity of $\sim$80 A W^{-1}, external quantum efficiency $\sim$24.8%, and a gain of $\sim$10^5 for a wavelength of 4 μms [95]. While the NIR InGaAs and Si platforms still dominate with quantum efficiencies exceeding 90%, this is impressive performance for the mid-IR [96].

Unfortunately, even with these advances, there are inherent physical limitations to the performance of photodetectors at longer wavelengths versus direct detection of shorter wavelengths. Antoni Rogalski has thoroughly documented the development of various high-operating temperature photodetector materials for several decades [93, 94, 97–99]. There are fundamental limits in detectivity as a function of

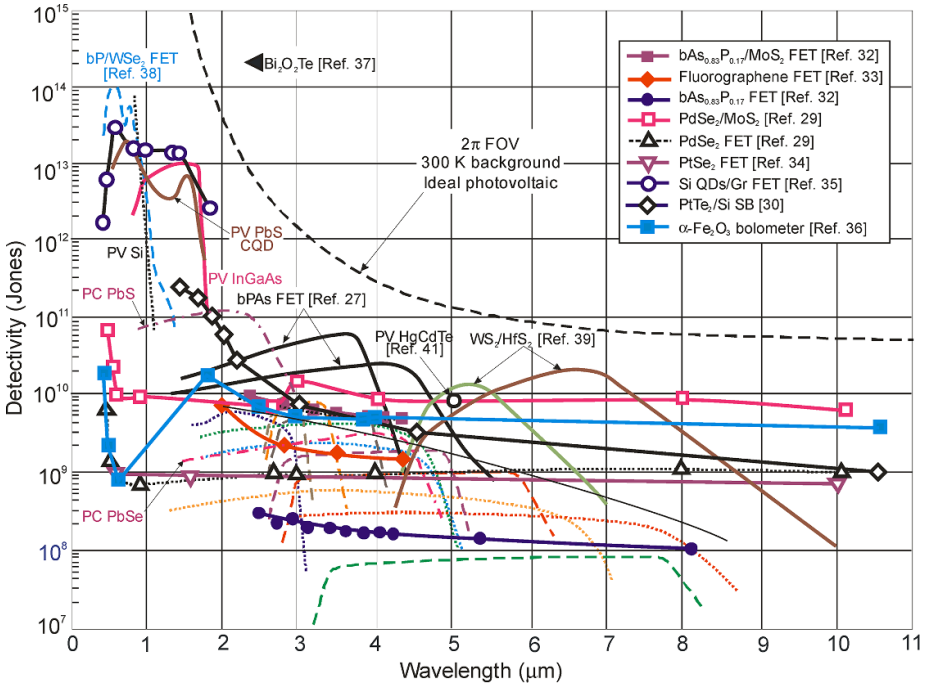

Figure 4. A plot of room-temperature spectral detectivity for a variety of materials pulled from recent literature. The acronyms stand for photoconductor (PC), photodiode (PV), and field-effect transistor (FET). Reproduced from [94]. CC BY 4.0.

wavelength for an ideal photodetector according to the background fluctuation limit, also known as BLIP (background limited infrared photodetector limit). This is due to the increase in background noise at room temperature for wavelengths longer than 1.2 μms [100]. In practical terms, maximum theoretical detectivity tends to decrease with increasing wavelength, which is illustrated in figure 4 from the literature review performed by Rogalski *et al* [94]. It is observed that the detector materials in the mid-infrared band are several orders of magnitude lower in detectivity than their NIR counterparts. This trend also holds with the dashed line indicated the theoretical ideal photovoltaic detector, which is a hard limitation due to the governing physics of photodetection. We recommend the cited literature from Rogalski and others for a more in-depth review of direct mid-infrared detection. The main takeaway for this review is that the theory suggests modern mid-IR materials will struggle to reach the performance of NIR devices due to physical limitations, regardless of advances in device technology.

Another consideration for mid-infrared technology is operating temperature. Even without the potential theoretical limitations on current detector materials, these devices operate best at a significantly lower temperature than comparable NIR devices. While there have been significant advances in high operating temperature detectors in the infrared, the smaller bandgap associated with mid-IR devices typically leads to increased dark currents that can only be mitigated by improved cooling (as low as ∼80 K) [101]. This is much lower than the typical operating temperature required for NIR SPADs at around 210–250 K, which can be accomplished with Peltier elements [102]. When considering the sensitivity required for quantum communication and other quantum applications with single-photon counting, we can safely consider this cooling to be mandatory if mid-IR SNR and link budgets are to be maximized. Even if parity in gain and noise behavior could be reached with the NIR, which is not the case as seen in figure 4, the cooling requirements increase device complexity, bulk, and operating costs compared to room temperature devices available in the NIR [47].

It is due to these limitations that nonlinear upconversion has gained popularity as a mid-IR detection tool. This involves using a nonlinear optical crystal to perform sum frequency generation, also known as frequency upconversion, to convert the mid-infrared photons into a shorter wavelength where the performance advantages of the NIR detectors can be leveraged. This method preserves the spatial, spectral, and quantum content of the mid-IR photons, and the only limitation on the detection range is the transparency region of the selected nonlinear crystal. Popular choices of nonlinear crystal include KTP, beta-barium borate (BBO), and $LiNbO_3$, with the latter having one of the larger transparency ranges at ∼350–5000 nm [103–105]. For those seeking longer wavelengths, there are also materials such as $AgGaS_2$ and $ZnGeP_2$, with transparency regions extending from the visible to >10 μms [106, 107]. There are also orientation-patterned semiconductors made using III–V materials like GaAs and GaP,

with transparency as high as 18 μms [108, 109]. However, the shorter wavelength materials (KTP, BBO, $LiNbO_3$) are well-established and can be consistently manufactured to a high-quality level. In contrast, longer wavelength materials are active areas of research and suffer from significant manufacturing difficulties that drive up costs and reduce crystal yields. As such, commercial off-the-shelf KTP or $LiNbO_3$ will be cheaper and easier to source compared to an orientation-patterned semiconductor or crystals like $ZnGeP_2$.

Outside of transparency, the main figure of merit for nonlinear crystals is the nonlinear coefficient, expressed in units of picometers/V. The nonlinear coefficient is determined by the polarization of the input light relative to the crystal axes and are described by the tensor coefficients of the nonlinear polarization tensor [110]. The higher the coefficient, the more efficient nonlinear optical processes will be in general. However, attempting to use a nonlinear crystal like this (referred to as perfect or birefringent phase matching) limits which crystals can be used for certain wavelengths. An alternative is to periodically pole the crystals via ferroelectric domain engineering. This allows use of any of the crystal's nonlinear coefficients with a multiplicative penalty of $2/\pi$. The tradeoff is typically worth it, as even with the penalty, the effective nonlinear coefficient is typically higher than the coefficient one would be forced to use with perfect phase matching. For some typical values, periodically poled KTP (PPKTP) has an effective nonlinear coefficient of $\sim$10.8 pm V^{-1}, while periodically poled lithium niobate (PPLN) has an effective nonlinear coefficient of $\sim$15 pm V^{-1} [111, 112].

The upconversion process has been well-documented, so a summary is provided here. Using the second order nonlinearity of the nonlinear medium, two input lasers can be combined in the medium to produce a unique output wavelength. In the case of upconversion, the output wavelength is determined by taking the sum of the individual photon energies of the two input lasers. As we must conserve energy and momentum, this is often expressed via the phase matching equation, which for upconversion is [110]:

$$\hbar k_3 = \hbar k_1 + \hbar k_2 \tag{1}$$

where $\hbar$ is the reduced Planck constant and is the wave vector for each wavelength (1 = pump, 2 = idler, 3 = signal). Typically, the pump beam is a high intensity laser around 1060–1080 nm, the idler is the incoming mid-IR photons to be detected, and the output signal will be $\sim$800 nm, although this will depend heavily on the selected mid-IR wavelength. To provide an illustrative example, if one were to mix 1064 nm and 3500 nm in the nonlinear crystal, the output wavelength would be $\sim$816 nm by the phase matching equation.

Now that the mechanics of upconversion are understood, the state of the art for upconversion can be investigated. The NIR was covered in a previous section, so here we focus only on advances using the 3–5 μm mid-IR atmospheric window. In the following section, we will discuss the quantum efficiency and SDE of the current record holders for mid-IR upconversion using a variety of schemes. The quantum efficiency for upconversion can be recovered by measuring the signal and idler power and converting it into a photon ratio:

$$\eta_{\text{upcon}} = \frac{P_s}{P_i}\frac{\lambda_i}{\lambda_s} \tag{2}$$

where represent the signal and idler power in watts, and $\lambda_{s,i}$ represent the signal and idler wavelengths. The overall SDE of the upconversion system (η_{tot}) is then given by considering the quantum efficiency of the NIR detector (η_{QE}), the upconversion quantum efficiency (η_{upcon}), and the losses due to optical coupling in the system (η_{opt}) [47]:

$$\eta_{\text{tot}} = \eta_{\text{opt}}\eta_{\text{upcon}}\eta_{\text{QE}}. \tag{3}$$

We will use η_{tot} as the main figure of merit for the upconversion detectors, and it will be calculated for the current record in the literature for each category of upconversion detector in the following section.

There have been numerous advances utilizing PPLN as the nonlinear medium due to its wide transparency range, high nonlinear coefficient, and the wide availability of high-quality off-the-shelf crystals. The current world record for continuous wave intracavity mid-IR upconversion is held by Dam *et al* in 2012, who demonstrated a quantum efficiency of 20% utilizing a Nd:YVO_4 based 1064 nm cavity enhanced pump to mix with a 2900–4200 nm idler [113]. Noise analysis showed that single-photon counting was easily attainable. Despite more than a decade having passed since this record was set, it has not been surpassed by any intracavity design so far to the best of our knowledge. However, a single pass

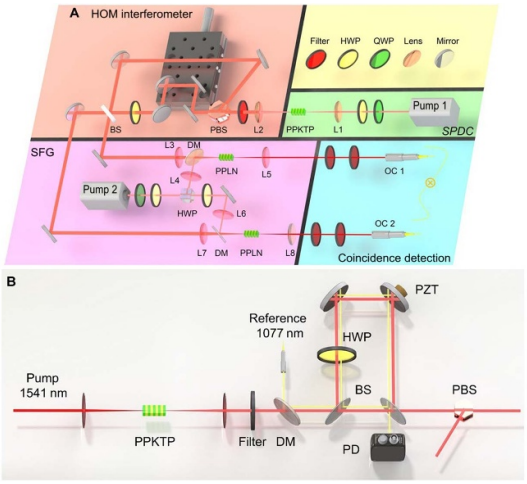

Figure 5. A schematic diagram of the entangled photon source and upconversion detection stages used by Ge *et al*. The pink and blue regions cover the upconversion detector, where the high energy pump is split into two branches to convert each photon of the entangled pair before coincidence detection. From [114]. Reprinted with permission from AAAS.

orientation developed by Ge *et al* recently in 2024 set a new continuous wave record with a quantum efficiency of 37.9% using 45 W 1077 nm pump light to upconvert 3082 nm entangled photon pairs generated via PPKTP SPDC [114]. The coupling efficiency into a single mode fiber was 79.8%, meaning the overall SDE assuming a silicon SPAD with 80% QE was used would be ∼24%. This system also has the benefit of having been directly used to measure time entangled photons in the mid-IR, showing its suitability for free-space quantum communication. The detection system by Ge *et al* is depicted in figure 5.

Outside of continuous wave upconversion detectors, pulsed systems have attained even higher conversion efficiencies with the added complexity of optimizing both temporal and spatial overlap in the nonlinear medium. In 2017, Wolf *et al* demonstrated quantum efficiencies in the mid-IR as high as 82%, although the application was gas sensing and not quantum communication [115]. A comparable efficiency was achieved in 2021 by Huang *et al* for photon counting with >80% quantum efficiency and an optical coupling efficiency of ∼57%, leading to a SDE of ∼37% for their pulsed setup and a noise equivalent power of $1.8 \times 10^{(-17)}$ W $\mathrm{Hz}^{-(1/2)}$ [116]. Waveguide devices are also being developed, although based on a review of the literature they are significantly less common than devices based on bulk nonlinear crystals. This may be due to the inherent difficulty of creating a waveguide that can confine such a wide range of wavelengths. To the best of our knowledge, the current state of the art was achieved with a PPLN ridge waveguide by Lehmann *et al* with a quantum efficiency of 16% for the pump power used (0.192 W) and a coupling efficiency of 50%, leading to an SDE of 8% [117]. Given that the quantum efficiency per watt of pump was ∼85%/W, higher pump powers and improved coupling could easily allow mid-IR waveguide devices that meet or even exceed the performance of the bulk crystal devices, and the authors anticipate significant developments in this field in the next 5–10 years.

2.2.3. Other detectors

The previous two technologies, SNSPDs and upconversion detectors, tend to dominate the state-of-the-art for quantum applications in terms of performance. While there are some alternatives that have been used for quantum applications, they appear to be too early in development to compete. As such, this section is a brief review of up-and-coming technologies to keep an eye on over the next decade or two, but they will not be included in the performance table at the end of the section.

Photovoltaic detectors are one possible avenue for mid-infrared detection. The general principle is a semiconductor photodetector with a band gap smaller than the energy of the incident photons, causing them to be absorbed and generate a measurable current. Russo *et al* covered the state of the art of photovoltaic detectors up to 2022 quite thoroughly [47]. The most sensitive system covered in Russo *et al*'s review was a HgCdTe-based photovoltaic detector from Gabbrielli *et al* [118]. In general, photovoltaic detectors could not compete with avalanche photodiodes in terms of sensitivity for single-photon applications. However, photovoltaic devices have the advantages of linear responses, simple structures, and lower noise levels, so if their sensitivity can be improved, they may be a promising alternative for some applications. Since Russo's review in 2022, a promising detector using BP and a van der Waals

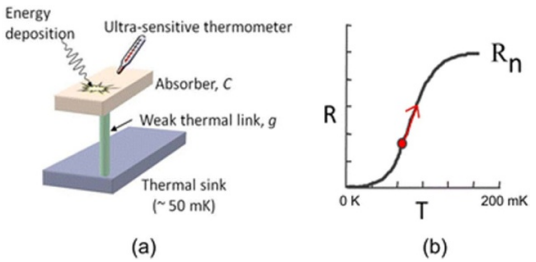

Figure 6. (a) Schematic diagram of a transition edge sensor. (b) Graph of the resistance versus temperature for the detector. The red arrow shows the change in resistance that is measured when a photon is incident on the absorber. Reproduced from [120]. CC BY 3.0.

probe was demonstrated by Abraham *et al* in 2024, with a SDE of 21.4% and a dark count of 720 Hz operating at room temperature [119]. However, this was for detection at 1550 nm, and it does not look like the device would be suitable for mid-infrared detection at this time. The authors of this review could not find any significant advances over the photovoltaic device reported by Gabbrielli *et al* operating in the mid-infrared in the literature.

Another alternative in the same vein as SNSPDs are transition edge sensors. These SPDs utilize the temperature-dependent resistance change near the superconductor critical temperature [120, 121]. As seen in figure 6, they are made up of an absorber, an ultra-sensitive thermometer, and a thermal sink.

The absorber is cooled to the superconducting transition temperature. When an incident photon is absorbed, the temperature change leads to a measurable change in absorber resistance. The temperature, and hence resistance, change is approximately proportional to the amount of energy absorbed, and therefore the TES can measure the number of photons in the incident pulse. This is in contrast to SPADs and SNSPDs, whose detection mechanisms are identically triggered regardless on the amount of absorbed energy. The main downside of these detectors are the complexity of measuring such low resistance values, slower response times than SNSPDs, and a typical operation temperature of $<$100 mK [120]. If these limitations can be addressed, the high optical efficiencies ($>$98%) could make them an attractive alternative to SNSPDs [122].

As a final up-and-coming detector, quantum dots could offer high detectivity for uncooled photodetection, although the current state of the art cannot compete with upconversion or SNSPDs. Colloidal quantum dots based on HgTe can be used to fabricate photodetectors with a high degree of tunability in the mid-infrared, with cut-off wavelengths ranging from 3–6 μms [123]. They also offer the potential to reduce costs for direct mid-IR detection, although currently they struggle with repeatability and quality issues as the understanding of growth mechanisms for HgTe is still being developed [124, 125]. A recent device presented by Caillas and Guyot–Sionnest in 2024 demonstrated a high detectivity of 9×10^9 Jones at room temperature using HgTe quantum dots and nanoantennas. While the SDE was not reported, the detectivity is in line with other high-end room temperature direct mid-infrared detectors in figure 3. This is still several orders of magnitude below the performance of the near-infrared however. It appears that, for now, quantum dots hold more promise as single-photon sources as opposed to SPDs, which is covered in more detail in section 3.

2.3. Space radiation and blinding attacks

The space environment presents a significant challenge for SPDs intended for satellite-based QKD. In Earth orbit, detectors are exposed to high fluxes of energetic protons and electrons from the Van Allen belts, solar energetic particles, and galactic cosmic rays. This radiation inflicts both ionizing dose and displacement damage (non-ionizing energy loss, NIEL) in the semiconductor lattice or supporting structure of SPDs, as well as generating secondary radiation in surrounding materials (bremsstrahlung). That environment must be accounted for and, where possible, mitigated when designing and operating a SPD payload on a satellite [126, 127].

For semiconductor-based SPADs, radiation-induced damage typically manifests as a large increase in DCR. Proton and neutron displacement damage create generation-recombination centers and traps in the depletion region, which leads to an increase in thermally-activated and trap-assisted noise. Studies have shown that SPADs irradiated to levels corresponding to months low Earth orbit show significant increases in DCRs. This increase in noise risks degrading the quantum bit error rate (QBER) of satellite-based demonstrations and thus reduce the secure key rate [128, 129]. The increased trap population also increases the afterpulse probability and timing jitter, and particularly heavy irradiation can cause

the dark count to increase so much as to saturate the readout electronics, preventing real single-photon signals from being detected.

By contrast, as covered above, SNSPDs offer inherently lower intrinsic dark counts, high detection efficiency and low timing jitter. However, SNSPDs are still vulnerable to radiation challenges in a space environment. Although displacement damage in the superconducting nanowire itself may be less of an issue than in semiconductors, high-energy particles (cosmic rays, secondary gamma radiation, neutrons) interacting in the substrate or surrounding materials can deposit energy, generate phonons or photons, and create bursts of quasiparticles in the nanowire. These bursts can produce erroneous transients, elevated count rates, or even temporary paralysis of the detector (dead time) as the superconducting state recovers. In addition, the cryogenic cooling system, readout electronics, and bias circuitry that are essential for SNSPDs must be qualified for total ionizing dose and single-event effects, adding complexity and risk to the mission [130–132]. Much of this complexity comes from the demands placed on spacecraft power and cooling mass due to the requirements of the cryogenic coolers involved. That being said, the authors found that literature quantifying the suitability of SNSPDs for deployment in space were limited, and this could represent a gap in the literature to be filled by the community in order to better compare SNSPDs to SPADs in high radiation environments.

Mitigation strategies for SPDs tend to focus on minimizing the dark count increases and maintaining the long-term sensitivity of the detector in the space environment. For SPADs, effective strategies include deep cooling and thermal annealing. By operating the detector at temperatures of −60 Celsius and lower, thermally generated carriers are heavily suppressed. Meanwhile, periodic annealing cycles at temperatures from 50–100 Celsius can reverse some of the displacement effects and recover dark count performance after irradiation [130, 133]. Other options include selecting small active-area or radiation-hardened SPADs, implementing shielding with low-Z materials to reduce proton and secondary particle flux, and using gated operation to limit the effective exposure window. Although the body of work on SNSPD radiation tolerance is more limited, a related study suggests that adding phonon-absorber layers can reduce energy transfer from high-energy particle hits, while shielding can limit cosmic-ray exposure [134]. Together, these approaches allow both detector types to maintain low DCRs and reliable performance despite the challenges of the space radiation environment.

Another consideration for satellite-based QKD are blinding attacks. Blinding attacks represent a significant hardware-level vulnerability in QKD systems making use of SPDs. In a blinding attack, an eavesdropper (Eve) illuminates the detectors used by Alice and Bob with intense continuous or pulsed light to force the detector out of single-photon sensitivity and into a less sensitive linear regime. Then, the Eve can selectively trigger the detectors to register the same measurement results the Eve has obtained. The Eve then listens to the classical channel and copies whatever Alice and Bob do in order to obtain the same secret key [135, 136]. As one might imagine, this is a significant risk and so proper mitigation techniques should be implemented to reduce the risk should such an attack occur. Before diving in to the mitigation techniques for these attacks, the authors must note that there are many types of attacks found in the literature besides the blinding attack: the after-gate attack, the dead-time attack, the time-shift attack, the superlinear attack, the device calibration attack, the double-click attack, and the back-flash attack, to name some. A full review of these attacks and mitigation strategies are beyond the scope of this review. However, the paper by Jiang *et al* includes a number of citations diving into these attacks in more detail for the interested reader [135]. This section is merely meant as a brief introduction to the concept of 'quantum hacking' and cover the blinding attack as one of the easier to implement attacks.

Blinding attacks on SPADs take advantage of the physics of the avalanche process. Under strong illumination, the diode's bias voltage can be driven below its breakdown threshold, causing the detector to transition from Geiger mode to a linear photodiode mode where the output current scales with optical power [137]. Temperature changes or increased dark counts from radiation exposure can modify the detector's breakdown voltage and threshold behavior, extending the range of illumination powers that can induce blinding [138]. In SNSPDs, blinding attacks rely on different physical mechanisms, but the end goal is the same: forcing the detector into a controllable or unresponsive state. Intense optical pulses can heat the superconducting nanowire above its critical temperature so that the device transitions into a resistive state. Under continuous illumination, the SNSPD can be latched in a blinded resistive condition. This leaves the SNSPD unable to respond to single photons, and Eve can trigger the SNSPD reliably once the bias current and thermal conditions have stabilized [139, 140]. Though SNSPDs can be more robust due to their cryogenic temperatures and lower bias margins, this still represents a possible attack pathway and must be monitored for in space-based QKD.

Mitigation strategies have been developed for both SPADs and SNSPDs to reduce the threat these attacks pose. For SPADs, optical power monitoring via the use of beam-splitters and a watchdog photodiode can track the incoming photon flux [141, 142]. Other strategies include randomized gating or self-differencing circuits that prevent predictable detection windows, and real-time bias current monitoring to detect illumination-induced shifts [135, 143]. Additionally, adopting measurement-device-independent (MDI) QKD architectures removes the need to trust individual detectors by performing Bell-state measurements jointly between Alice and Bob, removing the threat of detector-side attacks [144]. For SNSPDs, monitoring the nanowire bias current and voltage can help reveal latching or anomalous behavior from bright illumination. Adding optical power limiters at the receiver input can also prevent damaging or blinding optical flux from reaching the detector surface. Hardware diversity (using both SPADs and SNSPDs in the same receiver) has been proposed as another method to make receivers more resilient to blinding attacks given the differing responses to bright illumination [135, 139, 140, 145]. In conclusion, blinding attacks show that relying on the QKD protocols alone is insufficient to ensure QKD remains secure. For satellite-based QKD where *in-situ* modifications are not feasible, integrating such physical hardware-based mitigation strategies will be vital to ensuring such links remain secure as part of a global quantum communication network.

2.4. Detector performance table and conclusions

After reviewing the state-of-the-art in mid-IR single-photon counting, it is clear that the field has bridged the gap with the NIR at a rapid pace. We have collected the top performers for the detection technologies presented above in table 1. If SDE needs to be maximized at all costs, the best detectors are SNSPDs. At first glance, WSi would appear to be the most promising option, havingthe highest SDE reported at $>$50%. However, this value is from simulation work carried out by both Verma *et al* and Hampel *et al.* There appear to be no experimental confirmations of these optimized SDEs in literature, with work focusing on extending the cut-off wavelength of the saturated internal detection efficiency instead. This is a notable gap in the literature for mid-IR SNSPDs, and rigorous experimental work to verify WSi SDEs in the mid-infrared would be valuable. With this consideration, nonlinear upconversion appears to be the best option for mid-infrared SPD applications that have their SDEs validated by experimental demonstrations in the literature. Additionally, for practical applications, the cryo-cooling and fabrication requirements significantly increase the cost and complexity required for SNSPDs. As such, it may not be feasible to include the necessary infrastructure to hit the operating temperatures required for SNSPD operation. This may be less of a concern for terrestrial applications, but it is a notable potential setback for satellite-based applications, where access to cryo-cooling is significantly harder to guarantee. For higher temperature and cheaper detection payloads, nonlinear upconversion appears to be the best practical alternatives SNSPDs currently available that have mid-infrared experimental demonstrations of their SDEs in the literature.

When comparing these device efficiencies to comparable SNSPDs in the previous section, it is clear to see why mid-IR upconversion is considered one of the best current methods for detecting single mid-IR photons for quantum applications. Despite the efficiency and coupling penalties from the nonlinear process and additional optical components, the high performance of NIR detectors lead to detectors that outperform direct mid-infrared detectors on the market. Additionally, the upconversion efficiency continues to increase; there is no theoretical limit preventing quantum efficiencies as high as 99%, and the scientific community continues to produce improvements on existing designs. As coupling losses continue to be improved as well, we expect the detection efficiency record of $\sim$37% to slowly climb over time, and upconversion detectors could get close to performance parity with NIR single-photon counters for quantum communications. We can also see in table 1 that SDE for the pulsed setup demonstrated by Huang *et al* has actually exceeded the state-of-the-art for NbN SNSPDs and is on the same order of magnitude as the best SNSPD demonstrated in the mid-infrared to date. As such, one may assume upconversion will be the go-to solution in a wide variety of applications where room temperature operation and cost are the main concerns. The main challenge that upconversion should address is the DCRs, as they are still at least one order of magnitude higher than the average SNSPD, although the latter has demonstrated DCRs as low as one per day.

In terms of other figures-of-merit, it is notable that many of the cited examples did not include jitter or dead time values, especially in the mid-infrared. For upconversion detectors this is easier to understand, as the upconversion process can theoretically use any suitable detector in the wavelength range of the upconverted photons. Researchers may feel there is no point listing these values, as they are not specific to the upconversion method being reported but instead are specific to the model of detector being used. However, there was a notable lack of reporting of these values for the mid-IR SNSPDs as well. This improves somewhat when looking at the near-infrared SPADs and SNSPDs, although still roughly half of

Table 1. Summary of near-infrared and mid-infrared detector performance metrics.

Detector type	Material	Wavelength range (μm)	Internal quantum efficiency	System detection efficiency	Temperature (K)	Dark count rates (cps)	Timing jitter (ps)	Dead time	References
				Near-Infrared Detectors					
SNSPDs	NbN	1.53–1.63	100%	95%–98%	0.8–2.1	100	66	N/A	[146]
	NbTiN	1.29–1.5	100%	94%–99.5%	2.5–2.8	300–500	15–32	25 ns	[53]
	MoSi	1.55	100%	98%	0.7	N/A	N/A	N/A	[66]
APDs	InGaAs/InP	1.55	N/A	60%	300	340 000	N/A	3 ns	[48]
	InGaAs/InP	1.55	N/A	55.4%	250	43 800	N/A	N/A	[49]
	InGaAs/InP	1.55	N/A	25%	183	$<$200	$<$200	2–100 μs	[147]
	Silicon	780	N/A	70%	300	25–1500	N/A	22-50 ns	[46]
Upconversion	PPLN w/ SiSPAD	1550	N/A	40%	306	200	10–450	N/A	[51]
				Mid-Infrared Detectors					
SNSPDs	NbTiN	2-4	100%	84.1% @ 2 μm	0.76–2.2	$\sim$24 000	N/A	N/A	[73]
	NbN	1.5–10	100%	32.5% @ 2.95 μm	3.9	$<$100	N/A	N/A	[70]
	WSi	3.4–5.5	100%	$>$50% (simulated)	0.35	$<$1000	N/A	N/A	[83]
	MoSi	1.55–5.07	100%	N/A	0.085	$<$100	N/A	N/A	[85]
Upconversion (Pulsed)	PPLN w/ SiSPAD	3	$>$80%	37%	313	$\sim$1000	N/A	N/A	[116]
Upconversion (Continuous Wave)	PPLN w/ SiSPAD	3.082	37.9%	24%	300	N/A	N/A	N/A	[114]

the reported devices do not reference these values for the reported devices. One of the main takeaways from this review is that a concerted effort should be made by the research community to report these values alongside other metrics like SDE where possible, to better enable robust comparisons between different detector materials and architectures. For typical values, silicon and InGaAs/InP SPADs exhibit timing jitters in the tens to hundreds of picoseconds. A CMOS_integrated SPAD achieved ∼4 ps timing jitter at visible wavelengths [148]. However, it is more common to see SPADs with timing jitter on the order of 100 s of ps, such as this free-running InGaAs/InP device with 168 ps timing jitter [149]. By contrast, SNSPDs generally offer lower timing jitter, with single-digit ps values reported in the literature (2.6 ps in the visible and 4.3 ps at 1550 nm) by Korzh *et al* in 2020 [150]. In terms of dead time, SPADs can reach values in the tens of nanoseconds such as this SPAD that achieved a dead time of 28.5 ns in the visible, although InGaAs/InP SPADs dead times on the order of 1–10 μs in the near-infrared are more common [151, 152]. SNSPDs can also offer very short dead times in the near-infrared, with Miki *et al* demonstrating a dead time of 10 ns with a jitter of 45 ps in 2021, Zadeh *et al* reporting a dead time of <6 ns in 2020, while a comprehensive characterization from Dong *et al* in 2024 shows a dead time of 60 ns [153–155]. From the literature, we can conclude that SPADs tend to exhibit longer dead times and higher timing jitter versus SNSPDs in the near-infrared, and mid-infrared performance represents a gap in the literature that should be rectified going forward by more comprehensive reporting of detector performance in this wavelength region. Regardless, given the rapid improvement across both technologies, it is anticipated that the next decade will only see further improvement in these numbers, and parity with NIR single-photon counting may be achievable.

3. Probabilistic and triggered single-photon sources

An ideal single-photon source is one that deterministically emits indistinguishable single photons on demand, with no risk of multiphoton emission. It is characterized by exceptional photostability and precisely defined spatial and spectral properties, ensuring consistent and reliable performance in quantum information processing applications. From a quantum information perspective, deterministic on demand generation of indistinguishable single photons is an ideal resource for applications in quantum sensing [156], quantum metrology [157] and quantum information processing [158]. Such a source should have a sub-nanosecond lifetime and must be highly polarized in both emission and absorption [9]. Therefore, the wavelength of emitted photons should be well defined, the repetition rate of photon emission as high as possible, the probability of the single-photon emission should be equal to 1, with the probability of multi-photon emission is equal to 0. Realizing ideal single-photon sources in practice is extremely challenging due to the stringent requirements previously outlined. However, researchers have successfully developed promising candidates that satisfy several key criteria [159, 160]. The realistic single-photon sources can be divided into two groups—deterministic (on-demand) and probabilistic (or heralded). Each type of single-photon sources comes with its own set of advantages and disadvantages, making it impossible to identify a universally superior option for all conditions and circumstances. The choice of source is typically made with careful consideration of the specific requirements dictated by the target application. However, comparisons of the parameters across different types of sources can be found in various studies [9, 102, 161].

Probabilistic sources emit photon pairs with a probability less than unity. Heralded single-photon sources rely on the simultaneous generation of these photon pairs, where the detection of one photon is used to 'herald' the presence of the other. Although such sources can be driven at very high repetition rates, their per-excitation success probability is lower than that of other on-demand emitters. Photon-pair generation is typically achieved through SPDC or four-wave mixing (FWM). Both processes, however, carry a non-zero chance of producing multiple photon pairs, posing a security concern for QKD systems via photon-number-splitting attacks. Some of the earliest demonstrations of heralded single-photon sources used non-linear processes like SPDC to generate entangled photon pairs [162, 163]. In SPDC, a high-energy pump photon incident on a non-linear crystal can produce two lower-energy photons, commonly referred to as the signal and idler [164]. In contrast, FWM sources rely on third-order nonlinearities and can be realized in optical fibers or integrated waveguides due to improved mode confinement. Several reported implementations have shown that FWM-based sources can offer broader wavelength tunability and the potential for integration with photonic integrated circuits leveraging silicon technology [165–167].

Deterministic single-photon sources generate single photons through a triggered process, typically achieving higher single-photon emission rates due to their efficient operation. These sources are usually based on a two-level system that emits a photon after being excited. Various deterministic single-photon sources have been developed, including those involving molecules [168], nitrogen-vacancy (NV) centers

[169], and quantum dots [170–172]. The first experimental demonstration of single-photon emission was demonstrated by Kimble *et al* in 1977 using sodium atoms [173]. Since then, researchers around the world have demonstrated different techniques with similar characteristics, these include single molecules [173], and defect centers in solid state materials as diamond [174] and silicon carbide [175].

Next, we delve into the recent advancements in various types of single-photon sources, with a particular focus on those operating in the near-infrared spectrum, which are crucial for QKD applications [176, 177]. This review will cover the latest developments in both deterministic and probabilistic sources, examining their performance, efficiency, and suitability for secure quantum communication. Special attention will be given to the technical challenges and breakthroughs that have shaped the field, as well as the potential of such sources to enhance the reliability of QKD systems in real-world scenarios.

3.1. Coherent state sources

Coherent-state sources, such as weak coherent state and weak coherent pulse (WCP) sources, serve as the backbone of most current practical QKD demonstrations, including satellite-based implementations. In contrast to true single-photon sources such as those based on quantum dots, color centers, or SPDC and FWM, coherent-state sources rely on attenuated laser pulses whose photon number distribution is governed by Poissonian statistics [176, 178]. As the mean photon number per pulse can be precisely controlled, coherent state sources are relatively easy to implement and stable. This simplicity make them particularly suitable for space-based QKD missions, where compact size, power efficiency, and thermal stability are major considerations [179]. One drawback of coherent state sources is they have a non-zero probability of emitting multi-photon pulses, introducing a security vulnerability through photon-number-splitting attacks in which an Eve can capture extra photons without disturbing the quantum signal [180].

Single photon sources such as those previously covered avoid this multi-photon problem and thus offer improved security and potentially higher key rates per emitted photon under ideal conditions. However, they typically suffer from low collection efficiencies, limited brightness, and strict operational conditions like cryogenic cooling for quantum dots or the phase-matching conditions for SPDC/FWM crystals. In the context of satellite-based QKD where photon budgets are already constrained by link losses exceeding 30–40 dB, the low output rates of many single-photon sources can limit key throughput [27, 181, 182].

In contrast, coherent state sources offer orders-of-magnitude higher repetition rates (often GHz) and excellent beam quality, allowing for high-fidelity pointing and tracking in FSO channels. They remain an obvious choice for spaceborned QKD missions including the well-known Micius demonstration by China [179]. Security gaps from the multi-photon emission have been mitifated by decoy-state protocols, which statistically detect and eliminate photon-number-splitting attacks by varying the source intensity between signal and decoy pulses [183, 184]. As a result, modern decoy-state coherent source systems can approach the key rate and security performance of ideal single-photon sources. Recent practical examples have focused on space-oriented modular designs that target qualification and intensity modulation, such as the compact, iPOGNAC-based modular source targeting ∼800 nm with tunable signal/decoy intensities and polarization encoding specifically with space qualification in mind [185, 186]. Woodward *et al* have also pushed the boundaries of coherent state sources with very high clock rates, demonstrating gigahertz decoy-state and MDI QKD experiments, obtaining up to 8 bits per second at 54 dB channel loss and 2 kbps for 30 dB channel loss, with such demonstrations providing the building blocks for space downlinks and uplinks [187]. Practical space-payload implementations derived from these device capabilities have been described in payload studies that combine compact laser diodes, high-extinction modulators, and integrated random number generation to drive state selection, all while considering thermal environmental tolerances [188].

Compared with single-photon emitters and probabilistic photon-pair sources, modern coherent state sources have distinct tradeoffs relevant to satellites. They are far more mature and straightforward to space-qualify, routinely operate at much higher pulse rates (increasing raw key throughput under high loss), and pair readily with decoy-state protocols that largely close the photon-number-splitting vulnerability of Poissonian emission. However, they cannot produce truly on-demand single photons and therefore require careful intensity, spectral, and temporal calibration to avoid side channels that an Eve could exploit, although recent work has targeted these side channels for mitigation [189–191].

By contrast, triggered single-photon sources promise higher per-photon security and the potential for improved key-rate scaling in low-loss regimes, but current implementations tend to be heavier, less bright, or more environment-sensitive (requiring cryogenics or complex optical coupling) and therefore are still challenging to deploy on near-term small satellite missions.

3.2. Quantum dot based single-photon sources (700–1550 nm)

QDs, or the so-called artificial atoms, are semiconductor nanocrystals that can emit single photons when excited. They are often used due to their high brightness and ability to be integrated into photonic circuits. Common materials include InAs/GaAs, which can emit in the NIR range. Because of its quantum nature, a quantum dot has a discrete energy structure. When the dot is excited, either optically or electrically [192, 193], and in a weak-excitation regime where excitations are infrequent, an electron-hole pair is created. The radiative recombination of this pair leads to photon emission. While optical excitation can sometimes cause multi-photon emissions, the emitted photons will have different wavelengths. To address this, proper filtering is required.

Although quantum dots emit photons in all directions, making it challenging to collect them efficiently, this can be improved by integrating the quantum dot with a micro-cavity. Additionally, fabricating quantum dots using epitaxial growth on a prepared substrate is highly advantageous, as it facilitates miniaturization and integration into single-photon sources. However, to achieve optimal performance as a single-photon source, quantum dots typically need to operate at cryogenic temperatures [181].

InGaAs QDs are highly efficient, with generated photons achieving up to 96% indistinguishability and 99.4% purity [170, 194]. These QDs are created by embedding InAs within GaAs layers. The lattice mismatch between these materials causes strain, leading to the random formation of QDs on the surface through a process known as Stranski–Krastanov growth [195]. The difference in potential between the two materials creates a two-level system between for the electrons and holes, mimicking the behavior of artificial atoms despite being solid-state systems. This allows the QDs to emit single photons when excited and relaxed.

Single-photon sources that emit in the visible range are crucial for quantum information applications because visible light can pass through the Earth's atmosphere without significant absorption. Several promising QD systems are available for visible light emission at temperatures above 200 K. Deshpande *et al* [196] demonstrated anti-bunching up to 280 K, with $g^{(2)}(0)$ values of 0.37 under pulsed excitation and 0.32 under continuous excitation, using InGaN/GaN Stranski–Krastanov QDs emitting at 620 nm. $g^{(2)}(0)$ represents the probability of multiphoton emission events, where $g^{(2)}(0) = 0$ represents no probability of multiple photon emission as described by Chunnilall *et al* [9]. Similarly, Wang *et al* [197] achieved anti-bunching up to 220 K, $g^{(2)}(0) = 0.47$ with InGaN QDs grown on a non-polar crystal.

Single-photon emission in the visible spectrum has been demonstrated using II–VI QDs with CdSe QDs. Although CdSe QDs are often prepared in colloidal form, a few studies have focused on single-photon emission from epitaxial CdSe QDs systems. Rakhlin *et al* [198] reported anti-bunching with a $g^{(2)}(0)$ value of 0.15 at 80 K using CdSe/ZnSe Stranski–Krastanov QDs with a ZnSSe/ZnMgSSe barrier. Liu *et al* [32] observed anti-bunching with a $g^{(2)}(0)$ value of 0.4 at 100 K using CdSe/ZnSe QDs grown by molecular beam epitaxy. Fedorych *et al* [199] demonstrated room-temperature single-photon emission around 550 nm from CdSe/ZnSSe QDs embedded in a MgS barrier, with a $g^{(2)}(0)$ value of 0.16 under continuous wave excitation.

In [200], Gao *et al* reported applications of atomically thin single-photon sources based on transition metal dichalcogenides (TMDCs) for quantum communication, specifically focusing on a WSe2 monolayer. The WSe2 monolayer single-photon source exhibited high click rates of up to 66.95 kHz and anti-bunching values $g^{(2)}(0)$ as low as 0.034. The authors also used optimization techniques, such as temporal filtering, which allowed them to improve the performance further, extending the maximum tolerable transmission loss in the quantum channel by 3.51 dB. These metrics indicate a high purity of single-photon emission, essential for secure quantum communication.

In [201], Yang *et al* demonstrated QKD with a QD single-photon source in a 79 km link with a 25.49 dB loss (equivalent to 130 km in direct-connected optical fiber) between Hannover and Braunschweig in Germany. The setup achieved a record-high secret key bit rate of 4.8×10^{-5} per pulse with an average QBER of approximately 0.65%.

A similar approach of InAs QD single-photon source in photonic crystal waveguides for QKD applications has been demonstrated by Zahidy *et al* [202]. The authors used a link of 18 km between two districts in Copenhagen to realize QKD and achieved more than 2 kbits s^{-1} at approximately 10 dB channel loss.

In [203], Morrison *et al* demonstrated a fiber-based QKD technique with frequency-converted QD single photons at 1550 nm, achieving count rates of 1.6 MHz with $g^{(2)}(0)$ as low as 0.036 over 175 km of standard single mode fiber. The QD single-photon source used in this work emits photons at 940 nm, and excited using a dark-field confocal microscope. Another research demonstrated the use of QD single-photon source for QKD in the O-band, approximately at 1321 nm, in [204]. The authors achieved a raw key rate of up to 4.7 kHz, and $g^{(2)}(0)$ of 0.1. The single-photon source used consists of a single

InGaAs/GaAs QD that is integrated into a monolithic micromesa structure with a distributed Bragg-reflector mirror.

Demonstration of QKD using a QD single-photon source in an urban environment has been demonstrated in [205], achieving key rates of 106 bps during different environmental conditions. The single-photon source is fabricated using droplet etching epitaxy [206].

There have been numerous improvements in recent years in single-photon source capabilities. For example, Chaiwongkhot *et al* demonstrated a quantum dot single—photon source embedded in a nanowire that possessed very low multi-photon emission ($<10^{-6}$), and an extraction system efficiency of 3.1% [207]. Despite the low efficiency, the key generated by the quantum dot source is greater than that generated by a WCP source with an identical repition rate and link conditions simulating a satellite pass. They postulated that further improvements in extraction efficiency to a reasonable value of 40% would lead to the source outperforming the coherent state source by an order of magnitude. There have also been significant advances in novel solid-state platforms for single-photon sources. A review by Esmann *et al* covers the development of single emitters in monolayers of TMDCs, defects in hexagonal boron nitride, and colloidal quantum dots in perovskites, and benchmarks them versus other solid-state platforms for quantum photonics [208]. While the cited review covers these platforms in much more detail, the general outlook appears to be the brightness values and highly compact experimental demonstrations are highly promising for QKD demonstrations, although there are still issue with indistinguishability that prevent them from being used for protocols that require photon interference. From our review, the current experimental literature suggests that high-performance, pattern-mitigated coherent state sources with decoy-state control and GHz capability will remain the backbone of near-term satellite QKD demonstrations and mission designs. Meanwhile, continued development of deterministic single-photon emitters will aim to enable future mission classes once brightness, coupling efficiency and space-qualification are more mature.

While QD research has expanded across many spectral ranges, mid-IR QD-based single-photon sources (above 2 μm) remain unexplored. This absence may be due to challenges such as lack of mature materials and fabrication methods for efficient QD emission in the mid-IR, the complexity of integrating mid-IR QDs into photonic systems, and limited demand relative to NIR wavelengths, which align with existing fiber optics and telecom standards.

3.3. Color centers sources (600–1600 nm)

Color centers are another promising candidate for single-photon sources, notable for their ability to control the polarization of emitted photons [209]. These centers are based on defects in crystalline structures, most commonly NV in diamonds. NV centers exhibit a broad absorption and emission spectrum, with a central emission line around 637 nm [210]. Additionally, NV centers boast near-unity radiative efficiency, even at room temperature [211, 212]. Given their broad emission spectrum and the ability to fine-tune the output with appropriate spectral-line filters, color centers can serve as highly versatile and tunable photon sources for various quantum applications. The state-of-the-art of color centers sources is covered in [213].

3.4. SPDC or FWM sources (400–1300 nm)

SPDC sources utilize nonlinear optical materials that have non-zero elements in the second-order electric susceptibility tensor, known as $\chi^{(2)}$. These materials, which can include crystals and waveguides [158, 162], enable the conversion of a single pump photon into a pair of photons, commonly referred to as the signal and idler. The SPDC process was first theoretically predicted in 1961 [214] but was not experimentally observed until 1969 [215]. During SPDC, the pump photon is converted into a photon pair according to phase-matching conditions, which require the conservation of both energy and momentum. Depending on these phase-matching conditions, different types of SPDC processes are possible, each with distinct polarization characteristics. In type-0 SPDC, all three photons—pump, signal, and idler—have the same polarization. In type-I SPDC, the two generated photons share the same polarization, which is perpendicular to the polarization of the pump photon. In type-II SPDC, the two generated photons have perpendicular polarizations, while one of them shares the polarization of the pump photon. These variations in polarization properties allow SPDC sources to be tailored for specific quantum optical applications.

Early experiments aimed at producing polarization-entangled states often utilized BBO crystals with a Type-II SPDC process [216]. In this setup, the signal and idler photons are emitted in cones at different angles relative to the optic axis, resulting in two concentric rings at a given wavelength. To obtain a polarization-entangled state, photons must be collected from the points where these rings overlap. More

recent experiments have demonstrated significant advancements using a non-collinear scheme with periodically poled potassium titanyl phosphate (PPKTP) crystals. These setups have produced high-quality polarization-entangled states and exhibited strong two-photon interference visibility. Notably, Jeong *et al* [217] achieved a photon pair generation rate of 7000 pairs/mW and a Hong–Ou-Mandel (HOM) interference visibility of 97.8% for single-mode fiber and 93.6% for multimode fiber-coupled output modes. This experiment also showed that a broadband multimode diode laser could be effectively used as the pump source while still achieving high-quality two-photon interference, demonstrating the robustness and versatility of this approach for generating polarization-entangled states.

In [218], Lee *et al* reported a photon pair generation rate of 4200 pairs/mW and HOM interference visibilities exceeding 96%, depending on the pump power. Their setup also included a delay line, a half-wave plate, and a polarizing beam splitter to correct for temporal differences between photon pairs, which helped maintain high-quality entanglement and interference.

In [225], Fedrizzi *et al* reported a wavelength-tunable, fiber-coupled source of polarization-entangled photons using a 25 nm PPKTP crystal inside a Sagnac loop. This setup uses a polarizing beamsplitter to separate the clockwise and counterclockwise propagating signal and idler modes within the loop, resulting in a polarization-entangled state at the output. The system achieves a photon pair generation rate of 273 kHz mW nm^{-1} (with 82 kHz mW nm^{-1} detected) when coupled into single mode fibers and maintains high coincidence visibility across a broad tuning range of signal and idler wavelengths, exceeding 97.5% over approximately 50 nm. Furthermore, the Sagnac loop setup can be adapted for non-collinear phase matching, as demonstrated in [226], where Type-0 quasi-phase matching was employed to generate co-polarized photon pairs. This versatility and performance make the Sagnac loop scheme a powerful tool for generating entangled photon pairs in quantum communication and information processing applications.

In [26], Euler *et al* investigated entangled photon pair sources for QKD using type-II SPDC in a waveguide. The first source, they investigated, is driven by a 404 nm single-mode laser diode and operates around 808 nm, making it suitable for free-space QKD using the BB84 protocol. The PPKTP waveguides used are 4 mm and 11 mm long, with widths between a few micrometers. The second source is a fiber-based system optimized for QKD at telecom wavelengths near 1550 nm. It comprises of a 24 mm long PPLN waveguide. The key to advancing these technologies lies in understanding the spectral properties of the generated photons.

3.5. Mid-IR sources

Quantum optical systems working in the mid-IR wavelength range (3–5 μm) could bring major advancements in communications, sensing, and measurement technologies. However, most sources of entangled photons so far have been created in the near-IR range (700–1700 nm). Single-photon sources in the mid-IR range open the possibility of developing quantum technologies, like QKD, for mid-IR fiber communications and future earth-to-satellite communication systems. It is also important to note that mid-IR coherent state sources based on weak pulses like those covered in section 3.4 have not been reported in literature to the best of our knowledge. Recent efforts have focused mainly on the SWIR, which is understandable given the prior art and availability of high quality single photon detectors in that wavelength band. That being said, it does represent a significant gap in the literature, and the potential improvement in SNRs from the reduction in background radiation in the MWIR means that improved MWIR sources for QKD could lead to improved QBERs and key generation rates in the future. Table 2 summarizes some recent demonstrations of mid-IR QKD sources collected from the literature.

In [219], researchers used special lithium niobate crystals and advanced detectors to generate entangled photon pairs at 2090 nm. The reported coincidence-to-accidental ratio is around 180 ± 50 at 5 mW pump power. In general, near-IR (especially 1550 nm) is the most practical and widely used for current quantum technologies, while mid-IR is more promising for specialized applications, especially where atmospheric transmission or new sensing modalities are advantageous. Table 3 below summarizes some of the main qualitative characteristics of near- and mid-infrared single-photon sources as covered by this review.

Table 3 provides a comparative summary of the key features and challenges associated with single-photon sources in the mid-infrared (3–5 μm) and near-infrared (700–1700 nm) ranges. The goal of this comparison is to help readers identify the strengths, limitations, and applications of each spectral region, aiding the selection of appropriate sources for different quantum technologies. Near-IR technologies, especially around 1550 nm, benefit from well-developed telecom infrastructure, while mid-IR sources and components are still limited to research settings. Photon loss is much higher in mid-IR fibers, restricting its use for fiber-based quantum communication, whereas near-IR photons exhibit

Table 2. Mid-infrared single-photon sources from literature.

Source type	Wavelength range	Brightness	Coincidence-to-accidental ratio (CAR)	Reference
SPDC based on lithium niobate crystals	2–2.5 μm	N/A	180 $\pm$ 50 at 5 mW	[219]
Ultra-broadband bi-photon source	2.5–4.5 μm	106	N/A	[220]
PPKTP crystals	3–5 μm	N/A	N/A	[221]
Frequency up-conversion based on temporal-spectral quantum correlation	3–3.8 μm	N/A	60–100	[222]
SPDC in $AgGaS_2$ crystal	6 μm	N/A	22 at 2 mW	[223]
Four-wave mixing of low-power ultrashort laser pulses in a highly nonlinear fiber	N/A	106	N/A	[224]

Table 3. Summary of near-infrared and mid-infrared single-photon source characteristics.

Parameter	Mid-IR (3–5 μm)	Near-IR (700–1700 nm)
Common sources	Quantum cascade lasers (QCLs), SPDC, DFG, quantum dots, rare-Earth doped materials	Attenuated lasers, SPDC, quantum dots, nitrogen-vacancy (NV) centers
Photon loss in fiber	High in standard telecom fibers (especially >3 μm)	Low, especially at 1550 nm (0.2 dB km^{-1} in optical fibers)
Photon detection efficiency	Challenging, requires specialized detectors (e.g. TES, SNSPDs)	High, with optimized detectors like APDs and SNSPDs
Quantum applications	Emerging applications in quantum sensing, spectroscopy, and communication	QKD, quantum computing, and quantum communication
Component availability	Limited, mainly in research stage for quantum applications	Highly developed, telecom-ready components for 1550 nm
Energy per photon	Lower (since photons have lower energy in mid-IR)	Higher photon energy in the near-IR range

low attenuation, making them ideal for QKD and long-distance transmission. Photon detection in the mid-IR region is challenging, requiring specialized detectors (TES, SNSPDs), compared to the higher efficiency SPADs available in the near-IR. While near-IR sources are well-suited for QKD and quantum computing, mid-IR sources are gaining traction for quantum sensing, molecular spectroscopy, and free-space quantum communication.

4. Conclusions

After reviewing the state-of-the-art for mid-infrared SPDs and sources, there are some broad conclusions that can be made. First, mid-infrared SPDs are significantly more mature than mid-infrared single-photon sources. It was a struggle to find any literature that fully characterized mid-infrared single-photon sources using the typical figures of merit associated with entangled photon sources for quantum applications. It is clear that mid-infrared entangled photon sources are still in the early stages, and we expect that the next several years will see significant developments in this area due to the high interest in mid-infrared quantum applications. One clear area of improvement is in the reporting of empirical results for mid-infrared single-photon sources using the standard figures of merit, as this will better enable comparison with other sources in the literature and set benchmarks for the state-of-the-art as a whole. That being said, it is an exciting time for mid-infrared technology for single-photon emitters, as several recent high impact research articles cited in this review show the increasing attention and drive to innovate in this area.

The mid-infrared detectors are significantly more developed than the single-photon sources. This can likely be attributed to the need for high quality mid-infrared detectors for imaging applications that predate quantum applications, as many of the earlier works covered by this review do not explicitly mention quantum applications as the target for the developed technologies. The main difference between the near-infrared and the mid-infrared is the lack of suitable semiconductor photodiodes for direct detection in the mid-infrared. Materials like MCT and InSb simply cannot match the performance of current off-the-shelf silicon and InGaAs/InP SPADs. As a result, the only viable options in the

mid-infrared are SNSPDs or using frequency upconversion to convert the mid-infrared photons into the sensitivity range of the near-infrared semiconductor APDs. This has not proved to be a significant setback for mid-infrared SPDs, as table 1 in section 2.3 shows system detection efficiencies in the 30%–50% range. When compared to the near unity efficiencies of some near-infrared SNSPD detectors, this may not seem impressive, but the performance gains in the last decade have been pronounced. While we cannot say that mid-infrared SNSPDs have reached parity with their near-infrared counterparts, the performance gap is small enough that we may expect to see practical demonstrations of quantum communication, quantum sensing, and more in the mid-infrared region using this technology in the next 5–10 years. Frequency upconversion in particular seems promising for the mid-infrared, given the possibility for room temperature operation and current system detection efficiencies approaching that of upconverters in the near-infrared. With further refinement of the nonlinear conversion efficiency and by reducing losses elsewhere in the devices, we may see room temperature SPDs with small-to-no gap between them and the near-infrared alternatives.

In summary, the main roadblock for wide-scale testing of mid-infrared quantum technology is the lack of available single-photon sources. Once these have developed further and are more readily available to the scientific community, the detector technology is already mature enough to enable practical mid-infrared single-photon experiments. Given the high quality of existing mid-infrared SPDs coupled with the low background noise in the mid-infrared wavelength range, the mid-infrared could offer a compelling alternative with improved weather resistance to the current near-infrared standard in free-space quantum communications.

Data availability statement

No new data was created or analyzed in this study.

Acknowledgments

The authors would like to thank the Optical SatCom Consortium (OSC) and the National Research Council (NRC) of Canada for the support of the project.

Author contributions

Liam Flannigan 0000-0003-4694-419X
Conceptualization (equal), Investigation (equal), Methodology (equal), Validation (equal), Writing – original draft (equal), Writing – review & editing (equal)

Mostafa Khalil 0000-0003-4578-8535
Conceptualization (equal), Investigation (equal), Methodology (equal), Validation (equal), Writing – original draft (equal), Writing – review & editing (equal)

Phyllis Chiu
Conceptualization (supporting), Methodology (supporting), Validation (supporting), Writing – original draft (supporting)

Chang-qing Xu
Conceptualization (equal), Investigation (equal), Methodology (equal), Validation (equal), Writing – original draft (equal), Writing – review & editing (equal)

References

[1] Bayerstadler A 2021 Industry quantum computing applications *EPJ Quantum Technol.* **8** 1
[2] Bova F, Goldfarb A and Melko R G 2021 Commercial applications of quantum computing *EPJ Quantum Technol.* **8** 1
[3] Genovese M 2016 Real applications of quantum imaging *J. Opt.* **18** 073002
[4] Spitz O, Didier P, Durupt L, Diaz-Thomas D A, Baranov A N, Cerutti L and Grillot F 2022 Free-space communication with directly modulated mid-infrared quantum cascade devices *IEEE J. Sel. Top. Quantum Electron.* **28** 1–9
[5] Belenchia A 2022 Quantum physics in space *Phys. Rep.* **951** 1–70
[6] Pan D, Song X-T and Long G-L 2023 Free-space quantum secure direct communication: basics, progress, and outlook *Adv. Devices Instrum.* **4** 0004
[7] Krelina M 2021 Quantum technology for military applications *EPJ Quantum Technol.* **8** 1
[8] Adesso G, Bromley T R and Cianciaruso M 2016 Measures and applications of quantum correlations *J. Phys. A: Math. Theor.* **49** 473001
[9] Chunnilall C J, Degiovanni I P, Kück S, Müller I and Sinclair A G 2014 Metrology of single-photon sources and detectors: a review *Opt. Eng.* **53** 081910

[10] Guo-Yong X and Guang-Can G 2013 Quantum metrology *Chin. Phys. B* **22** 110601
[11] Zapatero V, van Leent T, Arnon-Friedman R, Liu W-Z, Zhang Q, Weinfurter H and Curty M 2023 Advances in device-independent quantum key distribution *npj Quantum Inf.* **9** 1–11
[12] Chen J-P *et al* 2021 Twin-field quantum key distribution over a 511 km optical fibre linking two distant metropolitan areas *Nat. Photon.* **15** 570–5
[13] Lu C-Y, Cao Y, Peng C-Z and Pan J-W 2022 Micius quantum experiments in space *Rev. Mod. Phys.* **94** 035001
[14] Yin J *et al* 2017 Satellite-based entanglement distribution over 1200 kilometers *Science* **356** 1140–4
[15] Pugh C J *et al* 2017 Airborne demonstration of a quantum key distribution receiver payload *Quantum Sci. Technol.* **2** 024009
[16] Jennewein T QEYSSat 2.0—White paper on satellite-based quantum communication missions in Canada vol 10 p 2024 (arXiv:2306.02481)
[17] Cai W-Q *et al* 2024 Free-space quantum key distribution during daylight and at night *Optica* **11** 647–52
[18] Li Y *et al* 2022 Space–ground QKD network based on a compact payload and medium-inclination orbit *Optica* **9** 933–8
[19] Gong Y-H *et al* 2018 Free-space quantum key distribution in urban daylight with the SPGD algorithm control of a deformable mirror *Opt. Express* **26** 18897–905
[20] Koushik C S N, Choubey S B, Choubey A and Pachori K 2020 A literature review on quantum experiments at space scale—QUESS satellite *Innovations in Electronics and Communication Engineering* ed H S Saini, R K Singh, M T Beg and J S Sahambi (Springer) pp 13–25
[21] Liao S-K *et al* 2017 Space-to-ground quantum key distribution using a small-sized payload on Tiangong-2 space lab* *Chin. Phys. Lett.* **34** 090302
[22] Chang L, Jiang H, Yang Y, Wu H, Wu Z and Cai J 2025 Coverage simulation of satellites Mozi and Jinan 1 during the quantum key distribution *J. Phys.: Conf. Ser.* **2977** 012095
[23] Vergoossen T *et al* 2020 SpooQy-1: the first nano-satellite to demonstrate quantum entanglement in space *Small Satellite Conf.* (available at: https://digitalcommons.usu.edu/smallsat/2020/all2020/10)
[24] Petermann T *et al* 2025 QUBE mission update: first year of operation of a 3U CubeSat for quantum-key-distribution experiments *76th Int. Astronautical Congress, IAC 2025* (*Sydney, Australien*) (available at: https://iafastro.directory/iac/proceedings/IAC-25/) (Accessed 11 November 2025)
[25] Heirich O *et al* 2025 EAGLE-1: qualification, calibration, and testing of the transmitter subsystem for Europe's first autonomous QKD system *76th Int. Astronautical Congress (IAC)* (*Sydney, Australien*) (available at: https://elib.dlr.de/216911/) (Accessed 11 November 2025)
[26] Euler S, Fitzke E, Nikiforov O, Hofmann D, Dolejsky T and Walther T 2021 Spectral characterization of SPDC-based single-photon sources for quantum key distribution *Eur. Phys. J. Spec. Top.* **230** 1073–80
[27] Bedington R, Arrazola J M and Ling A 2017 Progress in satellite quantum key distribution *npj Quantum Inf.* **3** 1–13
[28] Avesani M *et al* 2021 Full daylight quantum-key-distribution at 1550 nm enabled by integrated silicon photonics *npj Quantum Inf.* **7** 1–8
[29] Leitgeb E 2010 Analysis and evaluation of optimum wavelengths for free-space optical transceivers *2010 12th Int. Conf. on Transparent Optical Networks* pp 1–7
[30] Lanning R N, Harris M A, Oesch D W, Oliker M D and Gruneisen M T 2021 Quantum communication over atmospheric channels: a framework for optimizing wavelength and filtering *Phys. Rev. Appl.* **16** 044027
[31] Hadfield R H, Leach J, Fleming F, Paul D J, Tan C H, Ng J S, Henderson R K and Buller G S 2023 Single-photon detection for long-range imaging and sensing *Optica* **10** 1124–41
[32] Liu J J, Stann B L, Klett K K, Cho P S and Pellegrino P M 2019 Mid and long-wave infrared free-space optical communication *Proc. SPIE* **11133** 1113302
[33] Pavelchek A, Trissel R G, Plante J and Umbrasas S 2004 Long-wave infrared (10-micron) free-space optical communication system *Proc. SPIE* **5160** 247–52
[34] Flannigan L, Yoell L and Xu C 2022 Mid-wave and long-wave infrared transmitters and detectors for optical satellite communications—a review *J. Opt.* **24** 043002
[35] Er-long M, Zheng-fu H, Shun-sheng G, Tao Z, Da-sheng D and Guang-can G 2005 Background noise of satellite-to-ground quantum key distribution *New J. Phys.* **7** 215
[36] Hearne S 2023 Wavelength selection for satellite quantum key distribution *Masters* SETU Waterford (available at: https://repository.wit.ie/7712/)
[37] Temporao G, Zibinden H, Tanzilli S, Gisin N, Aellen T, Giovannini M, Faist J and von der Weid J 2008 Feasibility study of free-Space quantum key distribution in the mid-infrared *Quantum Inf. Comput.* **8** 1–11
[38] Wang Z, Malaney R and Green J 2019 Inter-satellite quantum key distribution at terahertz frequencies *ICC 2019–2019 IEEE Int. Conf. on Communications (ICC)* pp 1–7
[39] Ottaviani C, Woolley M J, Erementchouk M, Federici J F, Mazumder P, Pirandola S and Weedbrook C 2020 Terahertz Quantum Cryptography *IEEE J. Sel. Areas Commun.* **38** 483–95
[40] Liu C, Ye H-F and Shi Y-L 2022 Advances in near-infrared avalanche diode single-photon detectors *Chip* **1** 100005
[41] Ceccarelli F, Acconcia G, Gulinatti A, Ghioni M, Rech I and Osellame R 2021 Recent advances and future perspectives of single-photon avalanche diodes for quantum photonics applications *Adv. Quantum Technol.* **4** 2000102
[42] You L 2020 Superconducting nanowire single-photon detectors for quantum information *Nanophotonics* **9** 2673–92
[43] Yu C, Xu Q and Zhang J 2024 Recent advances in InGaAs/InP single-photon detectors *Meas. Sci. Technol.* **35** 122003
[44] Bienfang J, Gerrits T, Kuo P, Migdall A, Polyakov S and Slattery O T 2023 *Single-photon Sources and Detectors Dictionary* (National Institute of Standards and Technology (U.S.)) NIST IR 8486 (https://doi.org/10.6028/NIST.IR.8486)
[45] Hadfield R H 2009 Single-photon detectors for optical quantum information applications *Nat. Photon.* **3** 696–705
[46] Excelitas Technologies 2024 Single photonsingle-photon counting modules *Excelitas* vol 4 (available at: https://www.excelitas.com/product-category/single-photon-counting-modules) (Accessed October)
[47] Russo S D 2022 Advances in mid-infrared single-photon detection *Photonics* **9** 7
[48] Fang Y-Q, Chen W, Ao T-H, Liu C, Wang L, Gao X-J, Zhang J and Pan J-W 2020 InGaAs/InP single-photon detectors with 60% detection efficiency at 1550 nm *Rev. Sci. Instrum.* **91** 083102
[49] He T, Yang X, Tang Y, Wang R and Liu Y 2022 High photon detection efficiency InGaAs/InP single photonsingle-photon avalanche diode at 250 K *J. Semicond.* **43** 102301
[50] Sharma V and Bhardwaj A 2022 Analysis of differential phase shift quantum key distribution using single-photon detectors *2022 Int. Conf. on Numerical Simulation of Optoelectronic Devices (NUSOD)* pp 17–18

[51] Yao N et al 2020 Optimizing up-conversion single-photon detectors for quantum key distribution Opt. Express 28 25123–33
[52] Holzman I and Ivry Y 2019 Superconducting nanowires for single-photon detection: progress, challenges, and opportunities Adv. Quantum Technol. 2 1800058
[53] Chang J et al 2021 Detecting telecom single photonsingle-photons with 99.5−2.07+0.5% system detection efficiency and high time resolution APL Photon. 6 036114
[54] Raj V et al 2024 Advances in superconducting nanowire devices for UV to mid-infrared single-photon detection Proc. SPIE 5160 PC1302502
[55] Couteau C, Barz S, Durt T, Gerrits T, Huwer J, Prevedel R, Rarity J, Shields A and Weihs G 2023 Applications of single photons to quantum communication and computing Nat. Rev. Phys. 5 326–38
[56] Engel A, Renema J J, Il'in K and Semenov A 2015 Detection mechanism of superconducting nanowire single-photon detectors Supercond. Sci. Technol. 28 114003
[57] Laser 2000 (UK) Limited 2000 Cooled single photon detector array Laser (available at: https://photonics.laser2000.co.uk/products/light-detection-and-imaging/optical-receivers/photon-counting-and-timing/cooled-single-photon-detector-array/) (Accessed 11 November 2025)
[58] Wang L, Ye Y, Kong D, Bai T, Yao X, Yuan S, Zou P, Zhai W and Xia M 2025 Advances and perspectives in single photon detectors: principles, materials, cooling systems, and applications Adv. Opt. Mater. 13 2500138
[59] Miki S, Fujiwara M, Sasaki M and Wang Z 2009 Development of SNSPD system with Gifford-McMahon cryocooler IEEE Trans. Appl. Supercond. 19 332–5
[60] Chang J, Los J W N, Gourgues R, Steinhauer S, Dorenbos S N, Pereira S F, Urbach H P, Zwiller V and Esmaeil Zadeh I 2022 Efficient mid-infrared single-photon detection using superconducting NbTiN nanowires with high time resolution in a Gifford-McMahon cryocooler Photon. Res. 10 1063–70
[61] Dang H, Tan H, Zhang T, Zha R, Tan J, Zhao Y, Zhao B, Xue R and Li J 2021 A 1–2 K cryogenic system with light weight, long life, low vibration, low EMI and flexible cooling capacity for the superconducting nanowire single-photon detector IEEE Trans. Appl. Supercond. 31 1–5
[62] Hills M J et al 2019 A compact 4 K cooling system for superconducting nanowire single photon detectors IOP Conf. Ser.: Mater. Sci. Eng. 502 012193
[63] Renema J J et al 2014 Experimental test of theories of the detection mechanism in a nanowire superconducting single photonsingle-photon detector Phys. Rev. Lett. 112 117604
[64] Natarajan C M, Tanner M G and Hadfield R H 2012 Superconducting nanowire single-photon detectors: physics and applications Supercond. Sci. Technol. 25 063001
[65] Zhang T et al 2024 Superconducting single-photon detector with a speed of 5 GHz and a photon number resolution of 61 Photon. Res. 12 1328–33
[66] Reddy D V, Nerem R R, Nam S W, Mirin R P and Verma V B 2020 Superconducting nanowire single-photon detectors with 98% system detection efficiency at 1550 nm Optica 7 1649–53
[67] Korneev A, Korneeva Y, Florya I, Voronov B and Goltsman G 2012 NbN nanowire superconducting single-photon detector for mid-infrared Phys. Proc. 36 72–76
[68] Marsili F, Bellei F, Najafi F, Dane A E, Dauler E A, Molnar R J and Berggren K K 2012 Efficient single photonsingle-photon detection from 500 nm to 5 μm wavelength Nano Lett. 12 4799–804
[69] Marsili F, Najafi F, Dauler E, Bellei F, Hu X, Csete M, Molnar R J and Berggren K K 2011 Single-photon detectors based on ultranarrow superconducting nanowires Nano Lett. 11 2048–53
[70] Pan Y, Zhou H, Zhang X, Yu H, Zhang L, Si M, Li H, You L and Wang Z 2022 Mid-infrared Nb_4N_3-based superconducting nanowire single photonsingle-photon detectors for wavelengths up to 10 μm Opt. Express 30 40044–52
[71] Ma R et al 2024 Disorder enhanced relative intrinsic detection efficiency in NbTiN superconducting nanowire single photonsingle-photon detectors at high temperature Appl. Phys. Lett. 124 072601
[72] Taylor G G, MacKenzie E N, Korzh B, Morozov D V, Bumble B, Beyer A D, Allmaras J P, Shaw M D and Hadfield R H 2022 Mid-infrared timing jitter of superconducting nanowire single-photon detectors Appl. Phys. Lett. 121 214001
[73] China F, Yabuno M, Mima S, Miyajima S, Terai H and Miki S 2023 Highly efficient NbTiN nanostrip single-photon detectors using dielectric multilayer cavities for a 2-μm wavelength band Opt. Express 31 20471–9
[74] Karl P, Mennle S, Ubl M, Hentschel M, Flad P, Yang J-W, Peng T-Y, Lu Y-J and Giessen H 2022 Tunable infrared high absorbing polarization independent niobium nitride plasmonic perfect absorber nanowire photodetectors Opt. Mater. Express 12 2453–61
[75] Hao Z et al 2024 High-performance eight-channel system with fractal superconducting nanowire single-photon detectors Chip 3 100087
[76] Gu M, Zhang S, Wang X, Wang W, Liu D and Wu X 2024 Superconducting nanowire single-photon detector with polarization insensitivity, ultrafast response, and high efficiency Opt. Express 32 15537–45
[77] Banerjee A, Baker L J, Doye A, Nord M, Heath R M, Erotokritou K, Bosworth D, Barber Z H, MacLaren I and Hadfield R H 2017 Characterisation of amorphous molybdenum silicide (MoSi) superconducting thin films and nanowires Supercond. Sci. Technol. 30 084010
[78] Xie J and Zhang H 2024 Temporal and photon number resolution of superconducting nanowire single-photon detectors Appl. Phys. B 130 113
[79] Bao H et al 2021 Characterization of superconducting Nbn, WSi and MoSi ultra-thin films in magnetic field IEEE Trans. Appl. Supercond. 31 1–4
[80] Qin Z et al 2024 Thermal-property optimization dominated by the stoichiometric ratio in W-Si superconducting single-photon detectors Phys. Rev. Appl. 21 024046
[81] Baek B, Lita A E, Verma V and Nam S W 2011 Superconducting a-W_xSi_{1-x} nanowire single-photon detector with saturated internal quantum efficiency from visible to 1850 nm Appl. Phys. Lett. 98 251105
[82] Verma V B et al 2021 Single-photon detection in the mid-infrared up to 10 μm wavelength using tungsten silicide superconducting nanowire detectors APL Photon. 6 056101
[83] Hampel B, Mirin R P, Nam S W and Verma V B 2024 A 64-pixel mid-infrared single-photon imager based on superconducting nanowire detectors Appl. Phys. Lett. 124 042602
[84] Taylor G G, Walter A B, Korzh B, Bumble B, Patel S R, Allmaras J P, Beyer A D, O'Brient R, Shaw M D and Wollman E E 2023 Low-noise single-photon counting superconducting nanowire detectors at infrared wavelengths up to 29 μm Optica 10 1672–8
[85] Chen Q et al 2021 Mid-infrared single photonsingle-photon detector with superconductor $Mo_{0.8}Si_{0.2}$ nanowire Sci. Bull. 66 965–8

[86] Liu X, Xie B, Sun M and Jiao R 2024 Multispectral MoSi superconducting nanowire single photonsingle-photon detector *Opt. Commun.* **555** 130241
[87] Hu X 2024 Fractal superconducting nanowire single-photon detectors and their applications in polarimetric imaging *Proc. SPIE* **13025** 77–85
[88] Charaev I *et al* 2023 Single-photon detection using high-temperature superconductors *Nat. Nanotechnol.* **18** 343–9
[89] Charaev I *et al* 2024 Single-photon detection using large-scale high-temperature MgB_2 sensors at 20 K *Nat. Commun.* **15** 3973
[90] Merino R L, Seifert P, Retamal J D, Mech R K, Taniguchi T, Watanabe K, Kadowaki K, Hadfield R H and Efetov D K 2023 Two-dimensional cuprate nanodetector with single telecom photon sensitivity at T = 20 K *2D Mater.* **10** 021001
[91] Martyniuk P, Wang P, Rogalski A, Gu Y, Jiang R, Wang F and Hu W 2023 Infrared avalanche photodiodes from bulk to 2D materials *Light Sci. Appl.* **12** 212
[92] Li J, Dehzangi A, Brown G and Razeghi M 2021 Mid-wavelength infrared avalanche photodetector with AlAsSb/GaSb superlattice *Sci. Rep.* **11** 7104
[93] Rogalski A, Martyniuk P, Kopytko M and Hu W 2021 Trends in performance limits of the HOT infrared photodetectors *Appl. Sci.* **11** 2
[94] Rogalski A, Kopytko M, Hu W and Martyniuk P 2023 Infrared HOT photodetectors: status and outlook *Sensors* **23** 17
[95] Gao A *et al* 2019 Observation of ballistic avalanche phenomena in nanoscale vertical InSe/BP heterostructures *Nat. Nanotechnol.* **14** 217–22
[96] Wang B and Mu J 2022 High-speed Si-Ge avalanche photodiodes *PhotoniX* **3** 8
[97] Rogalski A 2022 Scaling infrared detectors—status and outlook *Rep. Prog. Phys.* **85** 126501
[98] Martyniuk P, Antoszewski J, Martyniuk M, Faraone L and Rogalski A 2014 New concepts in infrared photodetector designs *Appl. Phys. Rev.* **1** 041102
[99] Kopytko M and Rogalski A 2022 New insights into the ultimate performance of HgCdTe photodiodes *Sens. Actuators A* **339** 113511
[100] Rogalski A 2023 Overestimating the performance of photon detectors *Proc. SPIE* **12534** 78–91
[101] Kopytko M, Sobieski J, Gawron W and Martyniuk P 2022 Study of HgCdTe (100) and HgCdTe (111)B heterostructures grown by MOCVD and their potential application to APDs operating in the IR range up to 8 μm *Sensors* **22** 3
[102] Eisaman M D, Fan J, Migdall A and Polyakov S V 2011 Invited review article: single-photon sources and detectors *Rev. Sci. Instrum.* **82** 071101
[103] Leidinger M, Fieberg S, Waasem N, Kühnemann F, Buse K and Breunig I 2015 Comparative study on three highly sensitive absorption measurement techniques characterizing lithium niobate over its entire transparent spectral range *Opt. Express* **23** 21690–705
[104] Tamošauskas G, Beresnevičius G, Gadonas D and Dubietis A 2018 Transmittance and phase matching of BBO crystal in the 3−5 μm range and its application for the characterization of mid-infrared laser pulses *Opt. Mater. Express* **8** 1410–8
[105] Mamrashev A, Nikolaev N, Antsygin V, Andreev Y, Lanskii G and Meshalkin A 2018 Optical properties of KTP crystals and their potential for terahertz generation *Crystals* **8** 8
[106] Catella G C and Burlage D 1998 Crystal growth and optical properties of $AgGaS_2$ and $AgGaSe_2$ *MRS Bull.* **23** 28–36
[107] Verozubova G A, Gribenyukov A I, Vere A W, Flynn C and Ivanov Y F 2000 ZnGep2: optical transparency and melt composition *MRS Online Proc. Libr.* **607** 457
[108] Zheng D, Gordon L A, Wu Y S, Feigelson R S, Fejer M M, Byer R L and Vodopyanov K L 1998 16-μm infrared generation by difference-frequency mixing in diffusion-bonded-stacked GaAs *Opt. Lett.* **23** 1010–2
[109] Schunemann P G, Johnson K, Farrell C, Maidment L, Shi Y, Rutkauskas M and Reid D T 2021 Continuous wavelength tuning from 3.9–12 μm from an optical parametric oscillator based on orientation-patterned GaP grown on GaAs *Opt. Mater. Express* **11** 654–63
[110] Boyd R 2020 Nonlinear optics (Academic) (available at: https://shop.elsevier.com/books/nonlinear-optics/boyd/978-0-12-811002-7) (Accessed 26 September 2023)
[111] Niu Y, Yan X, Chen J, Ma Y, Zhou Y, Chen H, Wu Y and Bai Z 2022 Research progress on periodically poled lithium niobate for nonlinear frequency conversion *Infrared Phys. Technol.* **125** 104243
[112] Baozhen Z, Xiaoyan L, Yuxin L, Cheng W and Zhizhan X 2005 Investigation of noncollinear QPM optical parametric amplification based on periodically poled KTP *Opt. Commun.* **248** 387–94
[113] Dam J S, Tidemand-Lichtenberg P and Pedersen C 2012 Room-temperature mid-infrared single-photon spectral imaging *Nat. Photon.* **6** 788–93
[114] Ge Z *et al* 2024 Quantum entanglement and interference at 3 μm *Sci. Adv.* **10** eadm7565
[115] Wolf S, Trendle T, Kiessling J, Herbst J, Buse K and Kühnemann F 2017 Self-gated mid-infrared short pulse upconversion detection for gas sensing *Opt. Express* **25** 24459–68
[116] Huang K, Wang Y, Fang J, Kang W, Sun Y, Liang Y, Hao Q, Yan M and Zeng H 2021 Mid-infrared photon counting and resolving via efficient frequency upconversion *Photon. Res.* **9** 259–65
[117] Lehmann L, Grossard L, Delage L, Reynaud F, Chauvet M and Bassignot F 2019 Single photonSingle-photon MIR upconversion detector at room temperature with a PPLN ridge waveguide *Opt. Express* **27** 19233–41
[118] Gabbrielli T, Cappelli F, Bruno N, Corrias N, Borri S, De Natale P and Zavatta A 2021 Mid-infrared homodyne balanced detector for quantum light characterization *Opt. Express* **29** 14536–47
[119] Abraham N, Watanabe K, Taniguchi T and Majumdar K 2024 Room temperature single photonsingle-photon detection at 1550 nm using van der Waals heterojunction *Adv. Funct. Mater.* **34** 2406510
[120] Lau J A, Verma V B, Schwarzer D and Wodtke A M 2023 Superconducting single-photon detectors in the mid-infrared for physical chemistry and spectroscopy *Chem. Soc. Rev.* **52** 921–41
[121] Irwin K D and Hilton G C 2005 Transition-edge sensors *Cryogenic Particle Detection* ed C Enss (Springer) pp 63–150
[122] Lamas-Linares A, Calkins B, Tomlin N A, Gerrits T, Lita A E, Beyer J, Mirin R P and Woo Nam S 2013 Nanosecond-scale timing jitter for single photonsingle-photon detection in transition edge sensors *Appl. Phys. Lett.* **102** 231117
[123] Chang R, Yang H, Wu Z and Shen H 2024 Recent advances in mid-infrared photodetection based on colloidal quantum dots: challenges and possible solutions *Coord. Chem. Rev.* **500** 215539
[124] Green M, Wakefield G and Dobson P J 2003 A simple metalorganic route to organically passivated mercury telluride nanocrystals *J. Mater. Chem.* **13** 1076–8
[125] Goubet N *et al* 2018 Wave-function engineering in HgSe/HgTe colloidal heterostructures to enhance mid-infrared photoconductive properties *Nano Lett.* **18** 4590–7

[126] Smith D J 2024 Analyzing the effects of space radiation on semiconductor devices *Am. J. Pure Appl. Phys.* **5** 11–20
[127] Aukerman L W, Song Y, Vernon F L Jr, Evans G A and Wilcox J Z 1982 Radiation effects on semiconductor optical devices for space communications *Proc. SPIE* **328** 56–65
[128] Wilson B A, Miloshevsky A, Hooper D A and Peters N A 2021 Radiation-induced dark counts for silicon single-photon detectors in space *Phys. Rev. Appl.* **16** 064049
[129] Moscatelli F *et al* 2013 Radiation tests of single photon avalanche diode for space applications *Nucl. Instrum. Methods Phys. Res. A* **711** 65–72
[130] Harwit A *et al* 2025 Mitigating the effects of space radiation on single-photon avalanche diodes (SPADs) *Proc. SPIE* **13376** 25–40
[131] Ivanov H, Leitgeb E, Pezzei P and Freiberger G 2019 Experimental characterization of SNSPD receiver technology for deep space FSO under laboratory testbed conditions *Optik* **195** 163101
[132] Tan H *et al* 2024 A 1 K-class cryogenic system and its coupling with SNSPD for space applications *IEEE Trans. Appl. Supercond.* **34** 1–6
[133] Anisimova E, Higgins B L, Bourgoin J-P, Cranmer M, Choi E, Hudson D, Piche L P, Scott A, Makarov V and Jennewein T 2017 Mitigating radiation damage of single photon detectors for space applications *EPJ Quantum Technol.* **4** 1–14
[134] Karatsu K, Endo A, Bueno J, de Visser P J, Barends R, Thoen D J, Murugesan V, Tomita N and Baselmans J J A 2019 Mitigation of cosmic ray effect on microwave kinetic inductance detector arrays *Appl. Phys. Lett.* **114** 032601
[135] Jiang L *et al* 2024 Countermeasure against blinding attack for single-photon detectors in quantum key distribution *J. Semicond.* **45** 042702
[136] Stipčević M Preventing detector blinding attack and other strong light attacks on quantum key distribution by use of an explicit random number generator
[137] Lydersen L, Wiechers C, Wittmann C, Elser D, Skaar J and Makarov V 2010 Avoiding the blinding attack in QKD *Nat. Photon.* **4** 801
[138] Makarov V, Bourgoin J-P, Chaiwongkhot P, Gagné M, Jennewein T, Kaiser S, Kashyap R, Legré M, Minshull C and Sajeed S 2016 Creation of backdoors in quantum communications via laser damage *Phys. Rev. A* **94** 030302
[139] Elezov M, Ozhegov R, Goltsman G and Makarov V 2019 Countermeasure against bright-light attack on superconducting nanowire single-photon detector in quantum key distribution *Opt. Express* **27** 30979–88
[140] Tanner M G, Makarov V and Hadfield R H 2014 Optimised quantum hacking of superconducting nanowire single-photon detectors *Opt. Express* **22** 6734–48
[141] Yuan Z L, Dynes J F and Shields A J 2011 Resilience of gated avalanche photodiodes against bright illumination attacks in quantum cryptography *Appl. Phys. Lett.* **98** 231104
[142] Makarov V 2009 Controlling passively quenched single photon detectors by bright light *New J. Phys.* **11** 065003
[143] Sajeed S, Chaiwongkhot P, Bourgoin J-P, Jennewein T, Lütkenhaus N and Makarov V 2015 Security loophole in free-space quantum key distribution due to spatial-mode detector-efficiency mismatch *Phys. Rev. A* **91** 062301
[144] Lo H-K, Curty M and Qi B 2012 Measurement-device-independent quantum key distribution *Phys. Rev. Lett.* **108** 130503
[145] Fujiwara M, Honjo T, Shimizu K, Tamaki K and Sasaki M 2013 Characteristics of superconducting single photon detector in DPS-QKD system under bright illumination blinding attack *Opt. Express* **21** 6304–12
[146] Hu P, Li H, You L, Wang H, Xiao Y, Huang J, Yang X, Zhang W, Wang Z and Xie X 2020 Detecting single infrared photons toward optimal system detection efficiency *Opt. Express* **28** 36884–91
[147] ID Quantique ID230 infrared single-photon detector. ID quantique (available at: www.idquantique.com/quantum-detection-systems/products/id230/) (Accessed 31 October 2025)
[148] Nolet F, Parent S, Roy N, Mercier M-O, Charlebois S A, Fontaine R and Pratte J-F 2018 Quenching circuit and SPAD integrated in CMOS 65 nm with 7.8 ps FWHM single photon timing resolution *Instruments* **2** 19
[149] Wu W, Shan X, Long Y, Ma J, Huang K, Yan M, Liang Y and Zeng H 2023 Free-running single-photon detection via GHz gated InGaAs/InP APD for high time resolution and count rate up to 500 Mcount/s *Micromachines* **14** 437
[150] Korzh B *et al* 2020 Demonstration of sub-3 ps temporal resolution with a superconducting nanowire single-photon detector *Nat. Photon.* **14** 250–5
[151] Chen M *et al* 2020 Design and implementation of a compact single-photon counting module *Electronics* **9** 1131
[152] Losev A V, Zavodilenko V V, Koziy A A, Filyaev A A, Khomyakova K I, Kurochkin Y V and Gorbatsevich A A 2022 Dead time duration and active reset influence on the afterpulse probability of InGaAs/InP single-photon avalanche diodes *IEEE J. Quantum Electron.* **58** 1–11
[153] Miki S, Miyajima S, China F, Yabuno M and Terai H 2021 Photon detection at 1 ns time intervals using 16-element SNSPD array with SFQ multiplexer *Opt. Lett.* **46** 6015–8
[154] Dong S *et al* 2024 Establishing an end-to-end workflow for SNSPD fabrication and characterization *Sci. Rep.* **14** 30891
[155] Esmaeil Zadeh I *et al* 2020 Efficient single-photon detection with 7.7 ps time resolution for photon-correlation measurements *ACS Photonics* **7** 1780–7
[156] Pirandola S, Bardhan B R, Gehring T, Weedbrook C and Lloyd S 2018 Advances in photonic quantum sensing *Nat. Photon.* **12** 724–33
[157] Helversen M, Böhm J, Schmidt M, Gschrey M, Schulze J-H, Strittmatter A, Rodt S, Beyer J, Heindel T and Reitzenstein S 2019 Quantum metrology of solid-state single-photon sources using photon-number-resolving detectors *New J. Phys.* **21** 035007
[158] Chen J, Pearlman A J, Ling A, Fan J and Migdall A 2009 A versatile waveguide source of photon pairs for chip-scale quantum information processing *Opt. Express* **17** 6727–40
[159] Paesani S, Borghi M, Signorini S, Maïnos A, Pavesi L and Laing A 2020 Near-ideal spontaneous photon sources in silicon quantum photonics *Nat. Commun.* **11** 2505
[160] Shaik A B D and Palla P 2021 Optical quantum technologies with hexagonal boron nitride single photonsingle-photon sources *Sci. Rep.* **11** 12285
[161] Sinha U, Sahoo S N, Singh A, Joarder K, Chatterjee R and Chakraborti S 2019 Single-photon sources *Opt. Photon. News* **30** 32–39
[162] Burnham D C and Weinberg D L 1970 Observation of simultaneity in parametric production of optical photon pairs *Phys. Rev. Lett.* **25** 84–87
[163] Magde D and Mahr H 1967 Study in ammonium dihydrogen phosphate of spontaneous parametric interaction tunable from 4400 to 16 000 Å *Phys. Rev. Lett.* **18** 905–7
[164] Couteau C 2018 Spontaneous parametric down-conversion *Contemp. Phys.* **59** 291–304
[165] Ma C, Wang X and Mookherjea S 2018 Photon-pair and heralded single photon generation initiated by a fraction of a 10 Gbps data stream *Opt. Express* **26** 22904–15

[166] Fulconis J, Alibart O, O'Brien J L, Wadsworth W J and Rarity J G 2007 Nonclassical interference and entanglement generation using a photonic crystal fiber pair photon source *Phys. Rev. Lett.* **99** 120501
[167] Garay-Palmett K, U'Ren A B, Rangel-Rojo R, Evans R and Camacho-López S 2008 Ultrabroadband photon pair preparation by spontaneous four-wave mixing in a dispersion-engineered optical fiber *Phys. Rev. A* **78** 043827
[168] Lounis B and Moerner W E 2000 Single photons on demand from a single molecule at room temperature *Nature* **407** 491–3
[169] Babinec T M, Hausmann B J M, Khan M, Zhang Y, Maze J R, Hemmer P R and Lončar M 2010 A diamond nanowire single-photon source *Nat. Nanotechnol.* **5** 195–9
[170] Uppu R *et al* 2020 Scalable integrated single-photon source *Sci. Adv.* **6** 8268
[171] Michler P, Kiraz A, Becher C, Schoenfeld W V, Petroff P M, Zhang L, Hu E and Imamoglu A 2000 A quantum dot single-photon turnstile device *Science* **290** 2282–5
[172] Arakawa Y and Holmes M J 2020 Progress in quantum-dot single photonsingle-photon sources for quantum information technologies: a broad spectrum overview *Appl. Phys. Rev.* **7** 021309
[173] Kimble H J, Dagenais M and Mandel L 1977 Photon antibunching in resonance fluorescence *Phys. Rev. Lett.* **39** 691–5
[174] Kurtsiefer C, Mayer S, Zarda P and Weinfurter H 2000 Stable solid-state source of single photonsingle-photons *Phys. Rev. Lett.* **85** 290–3
[175] Castelletto S, Johnson B C, Ivády V, Stavrias N, Umeda T, Gali A and Ohshima T 2014 A silicon carbide room-temperature single-photon source *Nat. Mater.* **13** 151–6
[176] Bennett C H and Brassard G 2014 Quantum cryptography: public key distribution and coin tossing *Theor. Comput. Sci.* **560** 7–11
[177] Basset F B *et al* 2021 Quantum key distribution with entangled photons generated on demand by a quantum dot *Sci. Adv.* **7** 6379
[178] Scarani V, Bechmann-Pasquinucci H, Cerf N J, Dušek M, Lütkenhaus N and Peev M 2009 The security of practical quantum key distribution *Rev. Mod. Phys.* **81** 1301–50
[179] Liao S-K *et al* 2017 Satellite-to-ground quantum key distribution *Nature* **549** 43–47
[180] Brassard G, Lütkenhaus N, Mor T and Sanders B C 2000 Limitations on practical quantum cryptography *Phys. Rev. Lett.* **85** 1330–3
[181] Senellart P, Solomon G and White A 2017 High-performance semiconductor quantum-dot single-photon sources *Nat. Nanotechnol.* **12** 1026–39
[182] Aharonovich I, Englund D and Toth M 2016 Solid-state single-photon emitters *Nat. Photon.* **10** 631–41
[183] Wang X-B 2005 Beating the photon-number-splitting attack in practical quantum cryptography *Phys. Rev. Lett.* **94** 230503
[184] Lo H-K, Ma X and Chen K 2005 Decoy state quantum key distribution *Phys. Rev. Lett.* **94** 230504
[185] Berra F, Agnesi C, Stanco A, Avesani M, Cocchi S, Villoresi P and Vallone G 2023 Modular source for near-infrared quantum communication *EPJ Quantum Technol.* **10** 1–12
[186] Vallone G, Agnesi C, Avesani M and Villoresi P 2021 Polarization modulation method of photonic pulses for generating quantum cryptographic keys, and related polarization modulator (available at: https://patentscope.wipo.int/search/en/detail.jsf?docId=WO2021078723) (Accessed 11 November 2025)
[187] Woodward R I, Lo Y S, Pittaluga M, Minder M, Paraïso T K, Lucamarini M, Yuan Z L and Shields A J 2021 Gigahertz measurement-device-independent quantum key distribution using directly modulated lasers *npj Quantum Inf.* **7** 58
[188] Mendes P N, Teixeira G L, Pinho D, Rocha R, André P, Niehus M, Faleiro R, Rusca D and Zambrini Cruzeiro E 2024 Optical payload design for downlink quantum key distribution and keyless communication using CubeSats *EPJ Quantum Technol.* **11** 1–19
[189] Gnanapandithan A, Qian L and Lo H-K 2025 Hidden multidimensional modulation side channels in quantum protocols *Phys. Rev. Lett.* **134** 130802
[190] Kish S P, Thapa C, Sayat M, Suzuki H, Pieprzyk J and Camtepe S 2024 Mitigation of channel tampering attacks in continuous-variable quantum key distribution *Phys. Rev. Res.* **6** 023301
[191] Sharma T, Biswas A, Ramakrishnan J, Chandravanshi P and Singh R P 2024 Mitigating the source-side channel vulnerability by characterisation of photon statistics *J. Lightwave Technol.* **42** 3221–7
[192] Brokmann X, Giacobino E, Dahan M and Hermier J P 2004 Highly efficient triggered emission of single photonsingle-photons by colloidal CdSe/ZnS nanocrystals *Appl. Phys. Lett.* **85** 712–4
[193] Zwiller V, Aichele T, Seifert W, Persson J and Benson O 2003 Generating visible single photonsingle-photons on demand with single InP quantum dots *Appl. Phys. Lett.* **82** 1509–11
[194] Tomm N *et al* 2021 A bright and fast source of coherent single photonsingle-photons *Nat. Nanotechnol.* **16** 399–403
[195] Stranski I N and Krastanow L 1937 Zur Theorie der orientierten Ausscheidung von Ionenkristallen aufeinander *Mon.hefte Chem.* **71** 351–64
[196] Deshpande S, Frost T, Hazari A and Bhattacharya P 2014 Electrically pumped single-photon emission at room temperature from a single InGaN/GaN quantum dot *Appl. Phys. Lett.* **105** 141109
[197] Wang T, Puchtler T J, Zhu T, Jarman J C, Nuttall L P, Oliver R A and Taylor R A 2017 Polarisation-controlled single photonsingle-photon emission at high temperatures from InGaN quantum dots *Nanoscale* **9** 9421–7
[198] Rakhlin M V *et al* 2018 Single-photon emitter at 80 K based on a dielectric nanoantenna with a CdSe/ZnSe quantum dot *JETP Lett.* **108** 201–4
[199] Fedorych O, Kruse C, Ruban A, Hommel D, Bacher G and Kümmell T 2012 Room temperature single photonsingle-photon emission from an epitaxially grown quantum dot *Appl. Phys. Lett.* **100** 061114
[200] Gao T, Helversen M, Antón-Solanas C, Schneider C and Heindel T 2023 Atomically-thin single-photon sources for quantum communication *npj 2D Mater. Appl.* **7** 1–9
[201] Yang J *et al* 2024 High-rate intercity quantum key distribution with a semiconductor single-photon source *Light Sci. Appl.* **13** 150
[202] Zahidy M *et al* 2024 Quantum key distribution using deterministic single-photon sources over a field-installed fibre link *npj Quantum Inf.* **10** 1–6
[203] Morrison C L *et al* 2023 Single-emitter quantum key distribution over 175 km of fibre with optimised finite key rates *Nat. Commun.* **14** 3573
[204] Gao T *et al* 2022 A quantum key distribution testbed using a plug&play telecom-wavelength single-photon source *Appl. Phys. Rev.* **9** 011412
[205] Basset F B *et al* 2023 Daylight entanglement-based quantum key distribution with a quantum dot source *Quantum Sci. Technol.* **8** 025002
[206] Gurioli M, Wang Z, Rastelli A, Kuroda T and Sanguinetti S 2019 Droplet epitaxy of semiconductor nanostructures for quantum photonic devices *Nat. Mater.* **18** 799–810
[207] Chaiwongkhot P *et al* Enhancing secure key rates of satellite QKD using a quantum dot single-photon source

[208] Esmann M, Wein S C and Antón-Solanas C 2024 Solid-state single-photon sources: recent advances for novel quantum materials *Adv. Funct. Mater.* **34** 2315936
[209] Lutz J J, Duan X F and Burggraf L W 2018 Semiconductor color-center structure and excitation spectra: equation-of-motion coupled-cluster description of vacancy and transition-metal defect photoluminescence *Phys. Rev. B* **97** 115108
[210] Gieysztor M, Misiaszek M, Veen J, Gawlik W, Jelezko F and Kolenderski P 2021 Interaction of a heralded single photonsingle-photon with nitrogen-vacancy centers in a diamond *Opt. Express* **29** 564–70
[211] Pezzagna S and Meijer J 2021 Quantum computer based on color centers in diamond *Appl. Phys. Rev.* **8** 011308
[212] Mizuochi N *et al* 2012 Electrically driven single-photon source at room temperature in diamond *Nat. Photon.* **6** 299–303
[213] Andrini G *et al* 2024 Solid-state color centers for single-photon generation *Photonics* **11** 2
[214] Louisell W H, Yariv A and Siegman A E 1961 Quantum fluctuations and noise in parametric processes. I *Phys. Rev.* **124** 1646–54
[215] Ciuti C, Schwendimann P and Quattropani A 2001 Parametric luminescence of microcavity polaritons *Phys. Rev. B* **63** 041303
[216] Kwiat P G, Mattle K, Weinfurter H, Zeilinger A, Sergienko A V and Shih Y 1995 New high-intensity source of polarization-entangled photon pairs *Phys. Rev. Lett.* **75** 4337–41
[217] Jeong Y-C, Hong K-H and Kim Y-H 2016 Bright source of polarization-entangled photons using a PPKTP pumped by a broad-band multi-mode diode laser *Opt. Express* **24** 1165–74
[218] Lee S M, Kim H, Cha M and Moon H S 2016 Polarization-entangled photon-pair source obtained via type-II non-collinear SPDC process with PPKTP crystal *Opt. Express* **24** 2941–53
[219] Prabhakar S *et al* 2020 Two-photon quantum interference and entanglement at 2.1 μm *Sci. Adv.* **6** eaay5195
[220] Roeder F, Gnanavel A, Pollmann R, Brecht O, Stefszky M, Padberg L, Eigner C, Silberhorn C and Brecht B Ultra-broadband non-degenerate guided-wave bi-photon source in the near and mid-infrared (arXiv:2408.12203) (Accessed 1 October 2024)
[221] Vanselow A, Kaufmann P, Chrzanowski H M and Ramelow S 2019 Ultra-broadband SPDC for spectrally far separated photon pairs *Opt. Lett.* **44** 4638–41
[222] Cai Y, Chen Y, Xin X, Huang K and Wu E 2022 Mid-infrared single-photon upconversion spectroscopy based on temporal-spectral quantum correlation *Photon. Res.* **10** 2614–21
[223] Kumar M, Kumar P, Vega A, Weissflog M A, Pertsch T and Setzpfandt F 2021 Mid-infrared photon pair generation in $AgGaS_2$ *Appl. Phys. Lett.* **119** 244001
[224] Petrov N L, Fedotov A B and Zheltikov A M 2019 High-brightness photon pairs and strongly antibunching heralded single photons from a highly nonlinear optical fiber *Opt. Commun.* **450** 304–7
[225] Fedrizzi A, Herbst T, Poppe A, Jennewein T and Zeilinger A 2007 A wavelength-tunable fiber-coupled source of narrowband entangled photons *Opt. Express* **15** 15377–86
[226] Jabir M V and Samanta G K 2017 Robust, high brightness, degenerate entangled photon source at room temperature *Sci. Rep.* **7** 12613